Dynamics of Atmospheres and Oceans 76 (2016) 29–51

Contents lists available at ScienceDirect

Dynamics of Atmospheres and Oceans

journal homepage: www.elsevier.com/locate/dynatmoce

# The sensitivity of the regional coupled ocean-atmosphere simulations over the Intra-Americas seas to the prescribed bathymetry

Vasubandhu Misra [a,b,c,*], A. Mishra [a,b,c], Haiqin Li [d,e]

[a] Center for Ocean-Atmospheric Prediction Studies, Florida State University, Tallahassee, FL, USA
[b] Department of Earth, Ocean and Atmospheric Science, Florida State University, Tallahassee, FL, USA
[c] Florida Climate Institute, Florida State University, Tallahassee, FL, USA
[d] CIRES, University of Colorado, Boulder, CO, USA
[e] Earth System Research Laboratory, NOAA, Boulder, CO, USA

ARTICLE INFO

*Article history:*
Received 4 January 2016
Received in revised form 13 July 2016
Accepted 31 August 2016
Available online 1 September 2016

*Keywords:*
Coupled downscaling
Intra-Americas Seas
Warm pool
Loop Current
SST bias

ABSTRACT

This study examines the sensitivity of the coupled ocean-atmosphere climate of the Intra-Americas Seas (IAS; which includes the Gulf of Mexico and the Caribbean Sea) and parts of the western tropical and sub-tropical Atlantic Ocean to the prescribed bathymetry in three independent multi-decadal, high-resolution (15 km grid interval), regional coupled ocean-atmosphere model (RCM) integrations centered over the IAS. All of these RCM integrations with different prescribed bathymetries are forced by identical global atmospheric and oceanic reanalysis at the lateral boundaries. It is observed that the model integration with a smoother and coarser bathymetry in the region (RCM-C) results in more widespread sea surface temperature (SST) bias across the IAS. We also note that the bias displayed by the RCM-C simulation is analogous to the bias in the IAS ocean circulation of some Coupled Model Intercomparison Project version 5 (CMIP5) models.

The models with an intermediate bathymetry (RCM-I) and finest bathymetry (RCM-F) rectify the bias in ocean transport through the Yucatan Channel relative to RCM-C but display mixed results with respect to SST bias. The RCM-C integration uses a bathymetry with a shallower Yucatan Channel, which tends to produce unrealistically weak flow through the Yucatan Channel and a weak Loop Current. However, the stronger heat transport through the Yucatan Channel in RCM-F results in significant warming of the northwestern tropical Atlantic Ocean and associated weakening of the surface easterly atmospheric winds relative to the other RCM integrations. Due to the weaker surface wind-induced shelf currents, the area comprised of western Gulf of Mexico and southern Caribbean Sea have a severe cold SST bias over the IAS in RCM-F relative to either RCM-I or RCM-C. RCM-I on the other hand significantly warms the western Gulf of Mexico. RCM-I displays the least SST bias over the IAS and the ocean transport through the Yucatan Channel is most comparable to the ocean reanalysis.

We contend that RCM-I produces the most accurate simulation as a result of the coupled response to changes in bathymetry that optimizes the response of the modulation of the surface easterlies, which triggers sufficient ocean eddy activity in the western Gulf of Mexico and energizes the shelf currents. However, the uniform cold SST bias in the regional domain of all three simulations is also associated with a corresponding underestimation of the net

* Corresponding author.
*E-mail address:* vmisra@fsu.edu (V. Misra).

http://dx.doi.org/10.1016/j.dynatmoce.2016.08.007

heat flux into the ocean. The findings of this study clearly suggest that ameliorations of the SST bias in the IAS have their origins both in the atmospheric and oceanic components of the climate system.



## 1. Introduction

The Intra-Americas Seas (IAS), which includes the Gulf of Mexico (GoM) and the Caribbean Sea, is a major source of moisture for continental North America throughout the year (Ruiz-Barradas and Nigam, 2005; Mo et al., 2005; Wang et al., 2006; Chan and Misra, 2010; Misra et al., 2014). For example, Chang and Oey (2010a) assert that without the effects of the GoM, the U.S. "Corn Belt" region would not likely be so named. Even some of the most severe winter storms that affected the eastern United States originated in the GoM (Bosart and Lin 1984; Businger et al., 1990). Similarly, the ocean heat content in the IAS plays an important role in the intensity changes of several Atlantic tropical cyclones (Shay et al., 2000; Mainelli et al., 2008; Shay 2009; Rappaport et al., 2010). Therefore, the importance of the IAS in regulating the climate and weather over a major part of continental North America cannot be overemphasized.

The IAS is also a region that hosts a major fraction of the largest western hemisphere warm pool (Wang and Enfield, 2001). This Atlantic Warm Pool (AWP) is objectively defined as the area enclosed by 28.5 °C isotherm in the IAS region and in the western tropical and subtropical Atlantic Ocean (Wang and Enfield, 2001, 2003). The AWP is a seasonal feature that appears in the boreal summer season, which peaks in middle of summer and disappears by late fall or early winter (Lee et al., 2005; Misra et al., 2013, 2014). The size of the AWP exhibits distinct interannual (Wang and Enfield, 2001, 2003; Wang et al., 2006, 2008a) and decadal variability (Wang et al., 2008b; Zhang et al., 2012). Diagnostic studies of the surface heat budget from ocean reanalysis and Ocean General Circulation Model (OGCM) simulations suggest that the cloud radiative fluxes play a dominant role in the seasonal cycle and interannual variability of the AWP (Lee et al., 2007; Misra et al., 2013).

In a related study, Clement et al. (2005) showed that ocean dynamics play a very important role in sustaining the warm pool in the western Pacific Ocean. They showed that the ocean dynamics, through poleward Ekman transport with the compensatory underlying Sverdrup dynamics of equatorward geostrophic flow and linked by equatorial upwelling, negate the homogenizing effects of the atmospheric processes to sustain the warm pool in the tropical Pacific. While their study could be generalized for all tropical warm pools, the geography and the bathymetry of the IAS is too different from the tropical Pacific to exactly relate it to the AWP. For example, Liu et al. (2012a) suggested that the dominating terms in the upper ocean heat budget of the GoM are the contrasting warming tendency of the upper ocean heat transport and cooling tendency of the net surface atmospheric fluxes. Nonetheless, the ocean transport of heat into and out of the IAS is fundamental for the regulation of its SST (Jayne and Marotzke 2002; Chang and Oey 2010a,b; Liu et al., 2012b). The Loop Current essentially brings the warm and saline water from the equatorial Atlantic to the GoM (Chang and Oey, 2010b). It should be mentioned that the prevailing Loop Current that enters through the Yucatan Channel (YC) and exits through the Florida Straits represents the upper limb of the global thermohaline circulation in the North Atlantic, a major source of the Gulf Stream, and constitutes a major part of the western boundary current in the North Atlantic Subtropical Gyre (Schmitz and Richardson, 1991).

The purpose of this study is to demonstrate the sensitivity of model simulations of the IAS climate and its variations to changes in the prescribed ocean bathymetry in a regional coupled ocean-atmosphere model. Three regional model integrations that are identical to each other except for the bathymetry employed are analyzed for their differences in this study. The motivation for this study is presented in the following section, which discusses the bias over the IAS in contemporary global climate models. A brief discussion of the model is provided in Section 3. The experiment design is presented in Section 4. The model simulations are then compared with each other and with observations (where available) and reanalysis that are used in forcing the regional model in the results Section 5. This is followed in Section 6 with a discussion of the lessons learned from the regional model integrations and potential relation to the bias displayed by the global models. The summary and conclusions are presented in Section 7.

## 2. Bias in global climate models

Several studies have shown that invariably all current and earlier versions of Coupled ocean-atmosphere General Circulation Models (CGCMs) display a very cold bias in the IAS region resulting in much smaller AWPs than are observed (Misra et al., 2009; Kozar and Misra 2012; Liu et al., 2012a, 2013). In fact, Kozar and Misra (2012) showed that even the seasonal cycle of the AWP has significant errors in the 20th century simulations of the CMIP5 suite of models. Many of these studies point to erroneous cloud-radiative feedbacks as a potential cause for this rather systematic cold SST bias displayed by general circulation models.

A complementary theory for this pervasive cold bias in the IAS region displayed by the CGCMs suggests that it could also be a result of not resolving the ocean currents sufficiently in the region (e.g. Liu et al., 2013). There is a growing consensus that a grid spacing of 20 km or less is required at the very least to resolve the Loop Current and the eddies it spawns (Hurlburt and Thompson, 1980; Chérubin et al., 2005, 2006). Liu et al. (2012b, 2015) point to significant ocean circulation bias in the

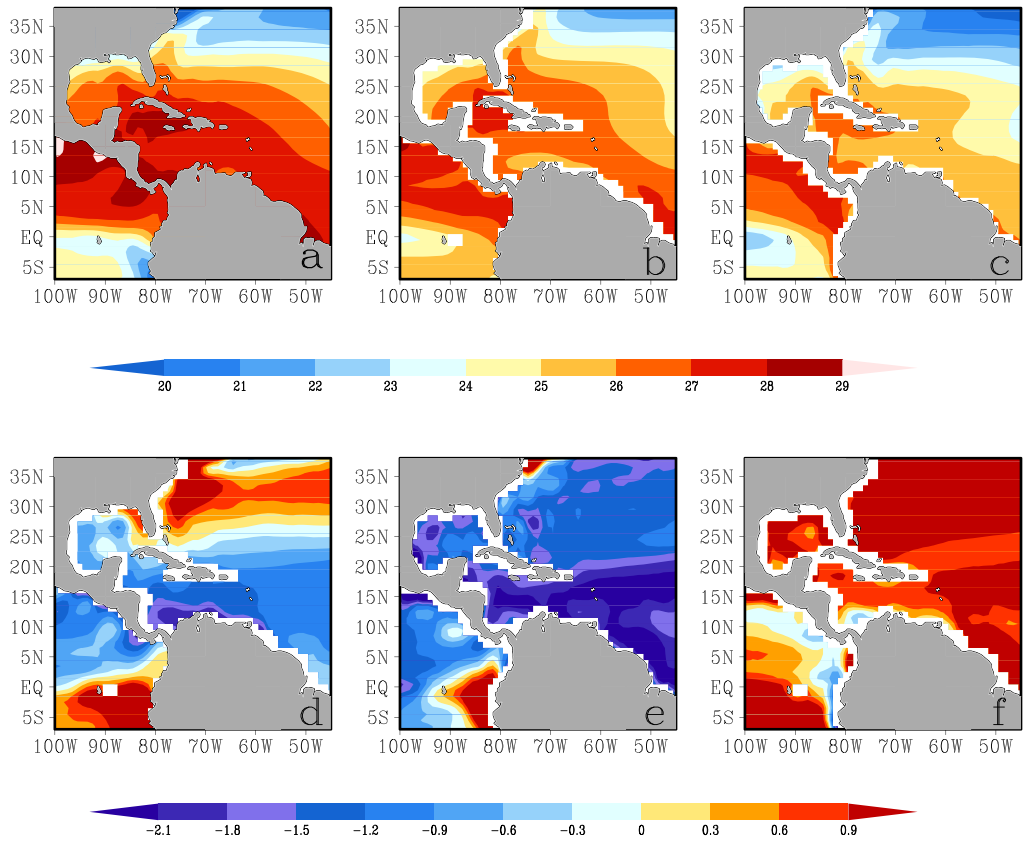


**Fig. 1.** Annual mean SST climatology from a) OISSTv2, and 20th century simulations from b) CCSM4, and c) GFDL-ESM2G. The corresponding SST bias from d) CCSM4, and e) GFDL-ESM2G. f) The difference in the annual mean climatology between CCSM4 and GFDL-ESM2G ([CCMS4]-[GFDL-ESM2G]) simulations. The units are in °C.

CMIP5 models over the IAS that potentially contribute to the cold bias in SST. To illustrate this, we show the annual mean climatology of SST and its bias from two of the CMIP5 20th century simulations in Fig. 1: CCSM4 (Gent et al., 2011) and GFDL-ESM2G (Dunne et al., 2012). Both of these model integrations are representative of the pervasive cold SST bias over the IAS that exists across the CMIP5 suite of models (Kozar and Misra, 2012). It should however be noted that, despite showing large differences in the magnitude of their cold SST bias (Fig. 1), the two CMIP5 models do not cover the range displayed by the rest of the CMIP5 models. Nonetheless, it is apparent that the cold bias in GFDL-ESM2G over the AWP region is far more severe than in the CCSM4.

The corresponding monthly mean volume flux through the YC from these two CMIP5 20th century simulations are presented in Fig. 2. For validation, we show the corresponding monthly mean volume flux from the Simple Ocean Data Assimilation version 2.2.4 (SODA; Carton and Giese, 2008). While this is not an ideal validation dataset, it is the closest proxy for observations of ocean transport through the YC available for ~100 years of the model simulations (1901–2005). SODA assimilates temperature and salinity profiles from the World Ocean Atlas (Mechanical Bathythermograph [MBT], Expendable Bathythermograph [XBT], Conductivity-Temperature-Depth Sonde [CTD], and station data), as well as additional hydrography, SST, and altimeter sea surface height anomalies (Carton and Giese, 2008). Moreover, SODA ocean reanalysis is generated by forcing the ocean model with ERA-40 daily atmospheric winds and QuikSCAT winds. Therefore there is a restraint on the model drift from both remote and local ocean observations that results in improved fidelity of SODA. In fact, the volume flux through the YC for a limited time (~5 years) observed from ocean moorings is comparable to the volume flux displayed in SODA ocean reanalysis (Candela et al., 2003; Athie et al., 2015; Fig. 2). Moreover, within these studies of non-overlapping observing periods there is a large disparity in the estimates of observed volume flux through the YC of over 10%, which is attributed to interannual variability (Athie et al., 2015). This called for the use of longer records for model validation of ocean volume flux through YC, which led us to apply data assimilated SODA ocean reanalysis.

The climatological monthly mean volume flux through the YC in CCSM4 (GFDL-ESM2G) is 31.72 Sv (15.85 Sv) while in the SODA ocean reanalysis it is 23.96 Sv (Fig. 2). These figures indicate large deviations in the ocean transport through the YC yielded by the two models. It may be noted that the size of the climatological AWP in CCSM4 is almost 60% more than that in the GFDL-ESM2G (Kozar and Misra, 2012), which may be partially a result of the stronger transport through the YC. Furthermore, both models incorrectly estimate the volume flux through YC, although GFDL-ESM2G displays slightly higher

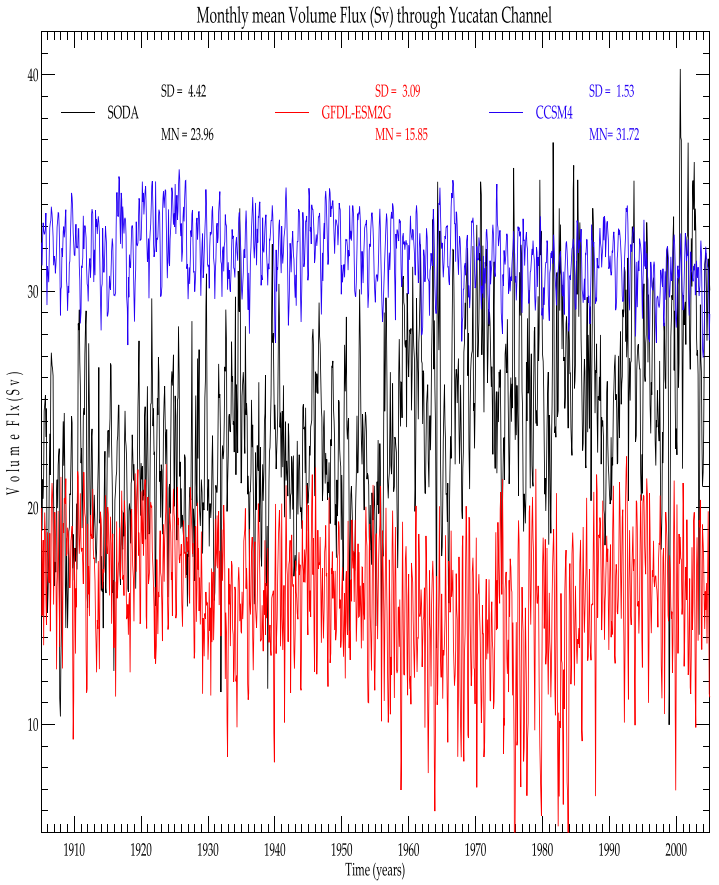


**Fig. 2.** The monthly mean volume transport (Sverdrups [Sv]) through the Yucatan Channel from GFDL-ESM2G and CCSM4 20th century simulations along with the SODA ocean reanalysis from SODA. The corresponding mean (MN) and standard deviation (SD) are also indicated.

variability than CCSM4. In Fig. 3 we show the corresponding heat transport through the YC from the two global models and the SODA ocean reanalysis. The heat flux (HF) through the channel is computed as:

$$HF = c_P \int_{Z_{bot}}^{Z_{surf}} \rho V_n \theta dz \tag{1}$$

where, $C_p$ is the heat capacity of seawater (=3993 J $Kg^{-1}$ $K^{-1}$), ρ is density of seawater, which follows from Jackett et al. (2006), $V_n$ is the component of the ocean current normal to the channel, and θ is the potential temperature. This figure clearly shows that the heat transported through the YC in CCSM4 (GFDL-ESM2G) is significantly over-estimated (under-estimated) relative to the SODA ocean reanalysis. However both global models considerably underestimate the size of the AWP relative to the observed SST analysis (Kozar and Misra, 2012) and display significant SST bias in the IAS (Fig. 1) despite this diverging bias of ocean heat transport through the YC (Fig. 3). This discussion clearly suggests that the global model bias in ocean circulation in the IAS is substantial. In this study we aim to analyze the response of the SST bias to changes in the IAS ocean circulation in a regional coupled ocean-atmosphere framework.

## 3. Model description

Here we provide a brief overview of the regional coupled ocean-atmosphere model (RCM), which follows from the Regional Spectral Model-Regional Ocean Modeling System (RSM-ROMS; Li and Misra, 2014). The reader is referred to Li et al. (2012) for a more detailed description of the model and the references therein. This model has been previously adopted in several other regional climate simulations (Li et al., 2012, 2013, 2014; Li and Misra 2014; Misra and Mishra 2016). The atmospheric component of the RCM is the RSM that has its origins in Juang and Kanamitsu (1994). It has gone through several updates and revisions and its most current version is described in Kanamitsu et al. (2010). The RSM has 28 terrain following sigma vertical coordinates. An outline of the physics used in the RSM for this study is provided in Table 1.

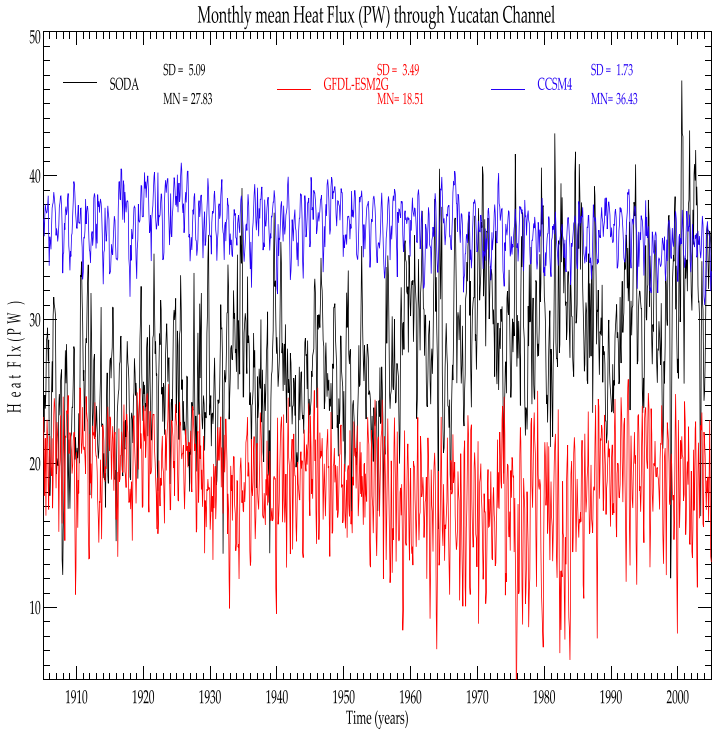


**Fig. 3.** Same as Fig. 2 for ocean heat transport (in PetaWatts [PW] = $10^{15}$ W) through the Yucatan Channel.

**Table 1**
Outline of the Regional Spectral Model (RSM) physics.

| Atmospheric Model (RSM) Physics | Reference |
|---|---|
| Land Model | Ek et al. (2003) |
| Longwave radiation | Chou and Suarez (1994) |
| Shortwave radiation | Chou and Lee (1996) |
| Deep convection | Moorthi and Suarez (1992) |
| Shallow convection | Tiedtke (1983) |
| Boundary layer | Hong and Pan (1996) |
| Gravity wave drag | Alpert et al. (1988) |

Similarly, the ROMS version 3.0 uses a stretched terrain following (S) coordinate for vertical discretization on a horizontal staggered Arakawa-C grid (Haidvogel et al., 2000; Shchepetkin and McWilliams, 2005). There are 30 sigma-levels in ROMS. The local closure scheme for mixing is based on the level 2.5 turbulent kinetic energy equations following Mellor and Yamada (1982) and generic length scale parameterization of Umlauf and Burchard (2003). The nonlocal closure scheme is based on the K-profile, boundary layer formulation developed by Large et al. (1994).

## 4. Experiment design

The regional domain over which the RCMs are integrated at 15 km grid interval is shown in Fig. 4. The three RCM integrations are conducted independent of each other but over identical domain and resolution (Fig. 4): The first integration, which follows the use of a smoother bathymetry, is RCM-C; The second, RCM-F, uses a finer bathymetry; and the third, RCM-I, has a bathymetry of intermediary realism between RCM-C and RCM-F. The bathymetries for all of these model integrations stem from ETOPO5 (http://www.ngdc.noaa.gov/mgg/global/etopo5.HTML), which is available at 5 min resolution. All three RCM simulations are conducted for a 32-year period from 1979 through 2010. They are forced at the lateral boundaries of the atmosphere with the 6 hourly atmospheric fields of the National Centers for Environmental Prediction-Department of Energy atmospheric reanalyis (NCEP-R2; Kanamitsu et al., 2002) and the monthly mean SODA ocean reanalysis as the lateral boundary forcing for ROMS.

We also use the SODA ocean reanalysis and the World Ocean Atlas (WOA; Locarnini et al., 2013) to compare with the multi-decadal RCM model integrations. Despite its prevalent uncertainties, the SODA ocean reanalysis serves as a good verification

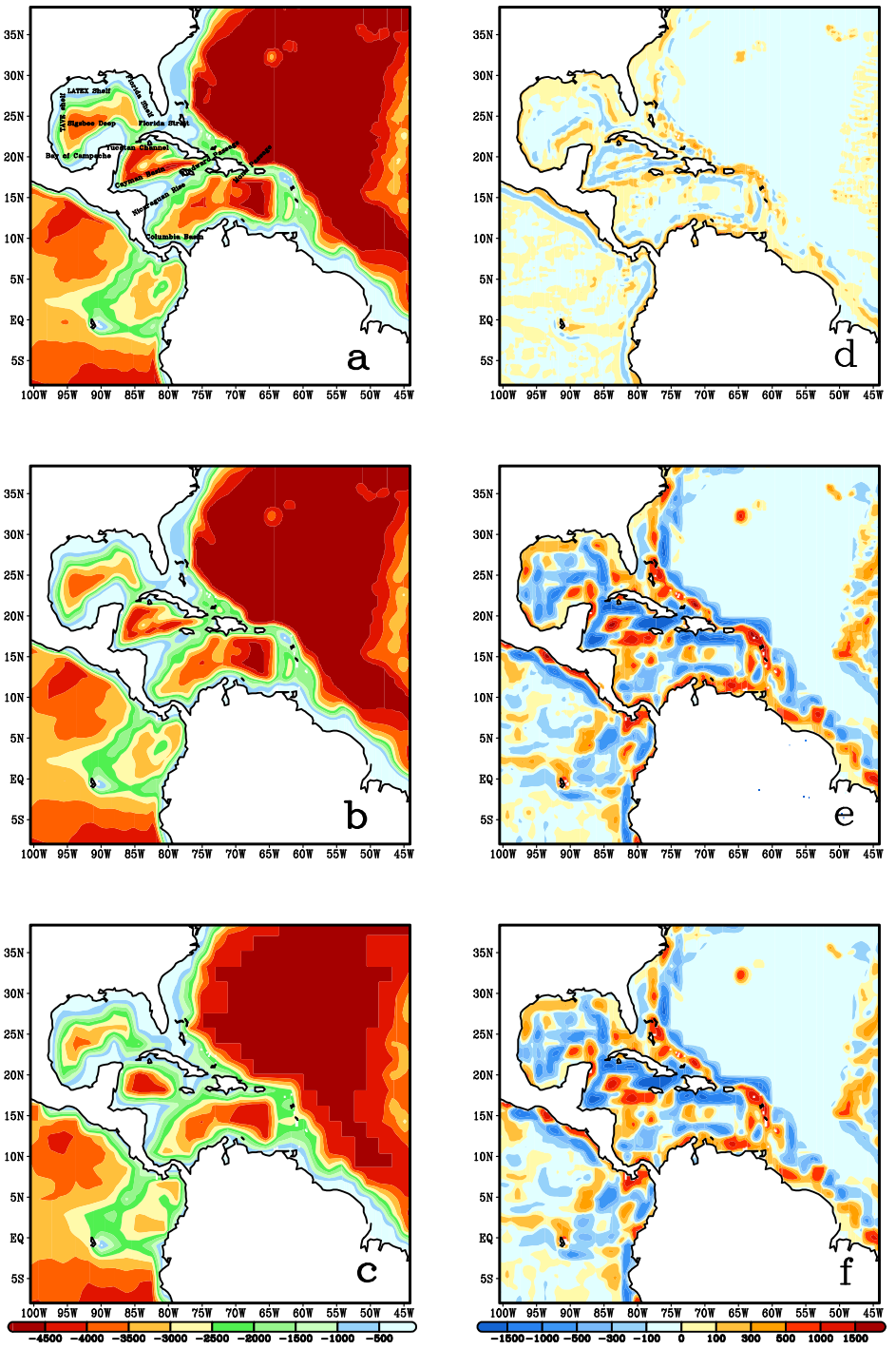


**Fig. 4.** The regional domain overlaid with bathymetry used in a) RCM-F with important features named, b) RCM-I, and c) RCM-C. The differences in bathymetry between them are shown in d) (RCM-F)-(RCM-I), e) (RCM-F)-(RCM-C), and f) (RCM-I)-(RCM-C). The units are in meters.

dataset given its availability for a relatively long time record (Giese and Ray, 2011). There are, however, extensive field programs such as CANEK (Sheinbaum et al., 2002) that have yielded useful information on the seasonal cycle and quantitative estimates of the discharge through the YC. But considering the uncertainty of the IAS from the natural variations (e.g. Loop Current variations; Leben, 2005; Dukhovskoy et al., 2014; Athie et al., 2015), we believe it is reasonable to use the data assimilated SODA ocean reanalysis to verify the ocean climate from the conducted multi-decadal model simulations. The WOA data available at 0.25° grid spacing is an objectively analyzed annual mean temperature profile using six decades of

data (1955–2012) available from the National Oceanographic Data Center and the World Data Center for Oceanography at standard depth levels from surface to a maximum depth of 5500 m (Locarnini et al., 2013). The initial conditions for RSM-ROMS are interpolated from the corresponding global atmospheric and oceanic reanalysis for 1 January 1979. These initial conditions are identical for all three RCM integrations, however we neglect the first five years of the model integration for the analysis of the results to account for spin-up issues. We use the 1984–2010 (27 year) period for the analysis of the results discussed in this paper.

In RCM-I, we smooth the bathymetry from ETOPO5 by first running a 5-point smoother prior to linearly interpolating to the 15 km grid of the ROMS; in the RCM-C, we linearly interpolate the original bathymetry to ∼200 km grid resolution (or T62 spectral truncation) before we interpolate it to the 15 km ROMS grid. The smoothing in the RCM-I is necessary to avoid numerical instability in the middle of the integration. The bathymetry for RSM-F is obtained by taking the average of the original ETOPO5 bathymetry and the bathymetry of RSM-I. The most notable impact of such a change is that the depth and extent of the continental shelf regions in RSM-F increases relative to RSM-I. In ROMS, which has a terrain following vertical coordinate system, the usual practice is to smooth the bathymetry to reduce errors in the computation of the horizontal pressure gradient (Mellor et al., 1994; Haidvogel et al., 2000; Martinho and Batteen 2006; Sikiric et al., 2009). Haney (1991) showed that ocean models with terrain following vertical coordinate system could have large errors in computing the horizontal pressure gradient, especially in regions of steep terrain. Therefore, based on the choice of the vertical coordinate system, the bathymetry may have to be altered to accommodate numerically stable solutions (Sikiric et al., 2009). More sophisticated approaches to smooth the bathymetry than what is adopted here do exist (Sikiric et al., 2009) and we will pursue these alternative methods in future studies. The differences in bathymetries (Fig. 4d–f) are apparent over several regions including: over the Colombian Basin, the Cayman Basin, the Nicaraguan Rise, the YC, the Sigsbee Deep, the Bay of Campeche, the Continental Shelf areas of the GoM, and over the Florida Straits (see Fig. 4a for their geographical location). In all of these regions the differences in the bathymetry range from a few meters to 1500 m or more. It should be noted that in Fig. 4e the YC in RCM-F is narrower in width and deeper in depth than in the RCM-C bathymetry. Furthermore, in Fig. 4e we see that the bathymetry in the Florida Straits between Florida and Cuba is deeper in RCM-F as compared to RCM-C. In addition, the continental shelf along Louisiana and Texas (known as the LATEX shelf) and along Tamaulipas-Veracruz in Mexico (the TAVE shelf) is deeper and extends further out in the GoM in RCM-C as compared to RCM-F. Similarly, the Windward and Mona passages are very shallow in RCM-C as compared to RCM-F. The differences between RCM-F and RCM-I (Fig. 4d) are comparatively smaller but share similar sign as the differences of bathymetry between RCM-F and RCM-C. Likewise, the differences between RCM-I and RCM-C (Fig. 4f) are similar in sign but larger in magnitude to those between RCM-F and RCM-I (Fig. 4d). However, an important difference is that the Windward and Mona passages in the bathymetry of RCM-F are a bit more realistic (and deeper) than that of RCM-I and RCM-C. As will be discussed in the following section, these differences in the bathymetry lead to some significant changes in the ocean simulation despite the identical grid resolution of RCM-C, RCM-I, and RCM-F.

For verification of the ocean surface currents we make use of the Ocean Surface Current Analysis (OSCAR; Bonjean and Lagerloef 2002; Helber et al., 2007), which is available at 1/3° grid resolution from 1993 to the present and is derived from satellite altimeter and scatterometer winds. It is worth noting that when comparisons of the model simulations are made with OSCAR it is based on the overlapping period (1993–2010) only. Similarly, we use the optimally interpolated SST version 2 (OISSTv2; Reynolds et al., 2007) available at 0.25°grid resolution for verification of the simulated SST. We also employ the Coordinated Ocean-ice Reference Experiments Phase 2 hindcast simulations (COREII; Large and Yeager, 2009) to verify the atmospheric fluxes from the model. COREII makes use of NCEP reanalysis for near surface meteorological fields along with a variety of satellite based radiation, SST, sea-ice concentration, and precipitation products to arrive at the atmospheric fluxes for the 1984–2006 period at 1° grid spacing. The balance of this paper's discussion focuses on the IAS and the western tropical and subtropical-Atlantic Ocean (AWP region) despite the fact that the regional domain covers parts of the tropical eastern Pacific Ocean.

## 5. Results

### 5.1. Ocean temperature

The climatological annual mean SST from RCM-F, RCM-I, and RCM-C are shown in Fig. 5a–c respectively. The relatively large-scale meridional gradient of the SST from the warm equatorial waters to the subtropical region of the Atlantic can easily be seen in all three panels. That said, significant biases along the coastal regions of the domain (e.g., over Bay of Campeche, the Florida Shelf, along the Mesoamerican coasts, the northern coast of South America, and along the southern limb of the Gulf Stream) are apparent (Fig. 5d–f). As evidenced in Fig. 5, all three RCM simulations display a pervasive cold SST bias over the IAS. However it is important to note that the SST bias along the coasts in Fig. 5d–f may also be partly on account of the differences in the resolution of the RSM-ROMS and OISSTv2. Nonetheless, Fig. 5h shows that for large portions of the IAS, the cold bias in RCM-C seems to be more acute than in RCM-F, especially along the southern limb of the Gulf Stream as well as over the Loop Current region of the GoM and in parts of tropical and subtropical western Atlantic Ocean. There are regions over the southern Caribbean Sea, along the LATEX shelf, along the northeast coast of GoM, and along western shelf of peninsular Florida where the RCM-C is warmer and depicts less bias than RCM-F (Fig. 5h). We note that RCM-I improved upon the cold bias of the RCM-F in the western GoM and over the southern Caribbean Sea (Fig. 5g). In the tropical western

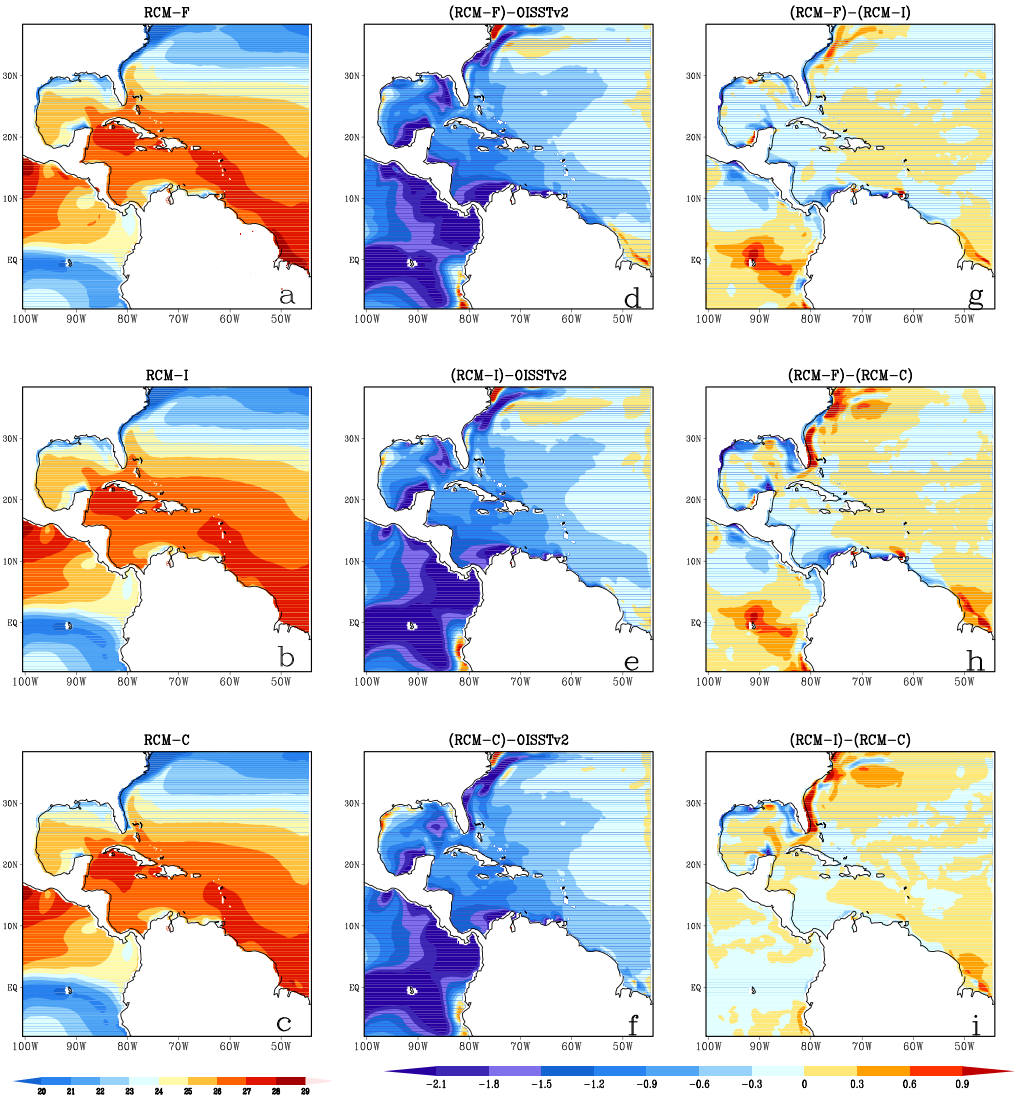


**Fig. 5.** The climatological annual mean SST (°C) from a) RCM-F, b) RCM-I, and c) RCM-C simulations. The corresponding SST bias (°C) from d) RCM-F (RCM-F-OISSTv2), e) RCM-I (RCM-I-OISSTv2), and f) RCM-C (RCM-C-OISSTv2) simulations. The difference in the climatological annual mean SST between g) RCM-F and RCM-I, h) RCM-F and RCM-C, and i) RCM-I and RCM-C simulations (°C).

Atlantic Ocean and along the Gulf Stream (off the coast of the Carolinas) the RCM-F is seen as an improvement over RCM-I (Fig. 5g).

The root mean square error (RMSE) of SST from RCM-F, RCM-I, and RCM-C relative to OISSTv2 are illustrated in Fig. 6a–c respectively. The differences between these RMSEs and the RCM simulations are shown in Fig. 6d–f. As mentioned with regards to Fig. 5, we see in Fig. 6 that RCM-F improves upon RCM-I and RCM-C over parts of the tropical and subtropical western Atlantic Ocean while RCM-I improves upon RCM-C and RCM-F over northern Caribbean Sea and western GoM (Fig. 6e and f). In other words, a more realistic bathymetry will not necessarily alleviate (and can even further deteriorate) the SST biases of a model simulation in isolated regions that could be emanating from other sources of model errors. These systematic differences in SST between RCM-F, RCM-I, and RCM-C merit further investigation. First, the different bathymetries are expected to change the circulation especially through the YC and other passages in the region. These changes will potentially provide a good source for investigation of the importance of ocean circulation on the regulation of SST over the IAS. Second, understanding the differences in the SST between RCM-F, RCM-I, and RCM-C, which is similar to the pervasive cold bias displayed over the IAS by Coupled General Circulation Models (CGCM's; Misra et al., 2009; Kozar and Misra 2012; Liu et al., 2012a,b, 2013), may provide some insights for improving future generations of CGCM.

In Fig. 7, a cross section along 25°N in the central GoM from RCM-F (Fig. 7a) and its corresponding differences with RCM-I (Fig. 7c), RCM-C (Fig. 7e) can be seen. Similarly, the corresponding observed cross section from WOA (Fig. 7b) and the systematic errors in RCM-F (Fig. 7d), RCM-I (Fig. 7f), and RCM-C (Fig. 7h) can also be seen. The figure clearly indicates

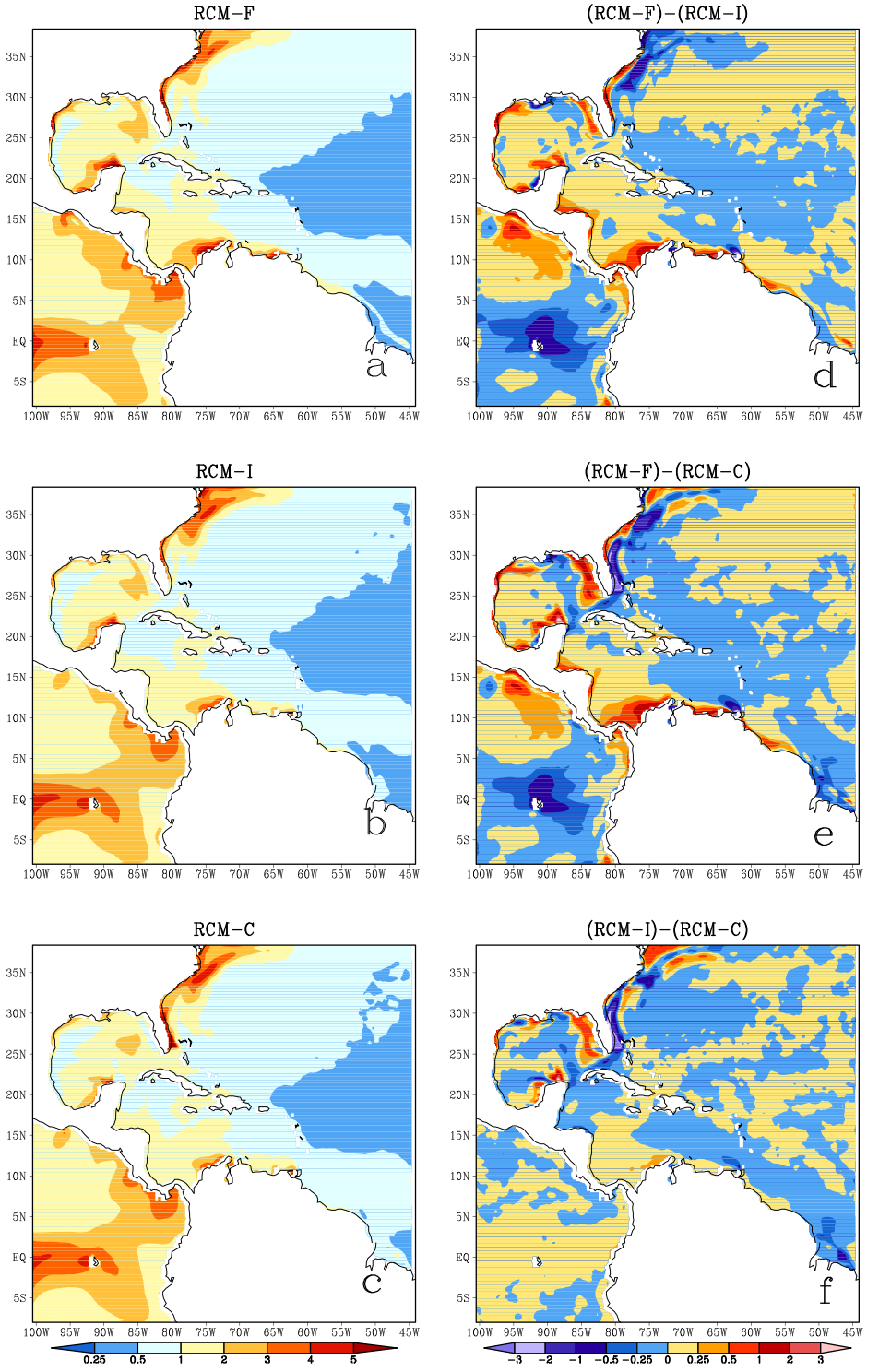


**Fig. 6.** The root mean square error (RMSE) of the climatological annual mean SST from a) RCM-F, b) RCM-I and c) RCM-C simulations. The corresponding differences of RMSE between d) RCM-F and RCM-I, e) RCM-F and RCM-C and f) RCM-I and RCM-C. and c) their corresponding RMSE difference (RCM-C-RCM-F). The units are in °C.

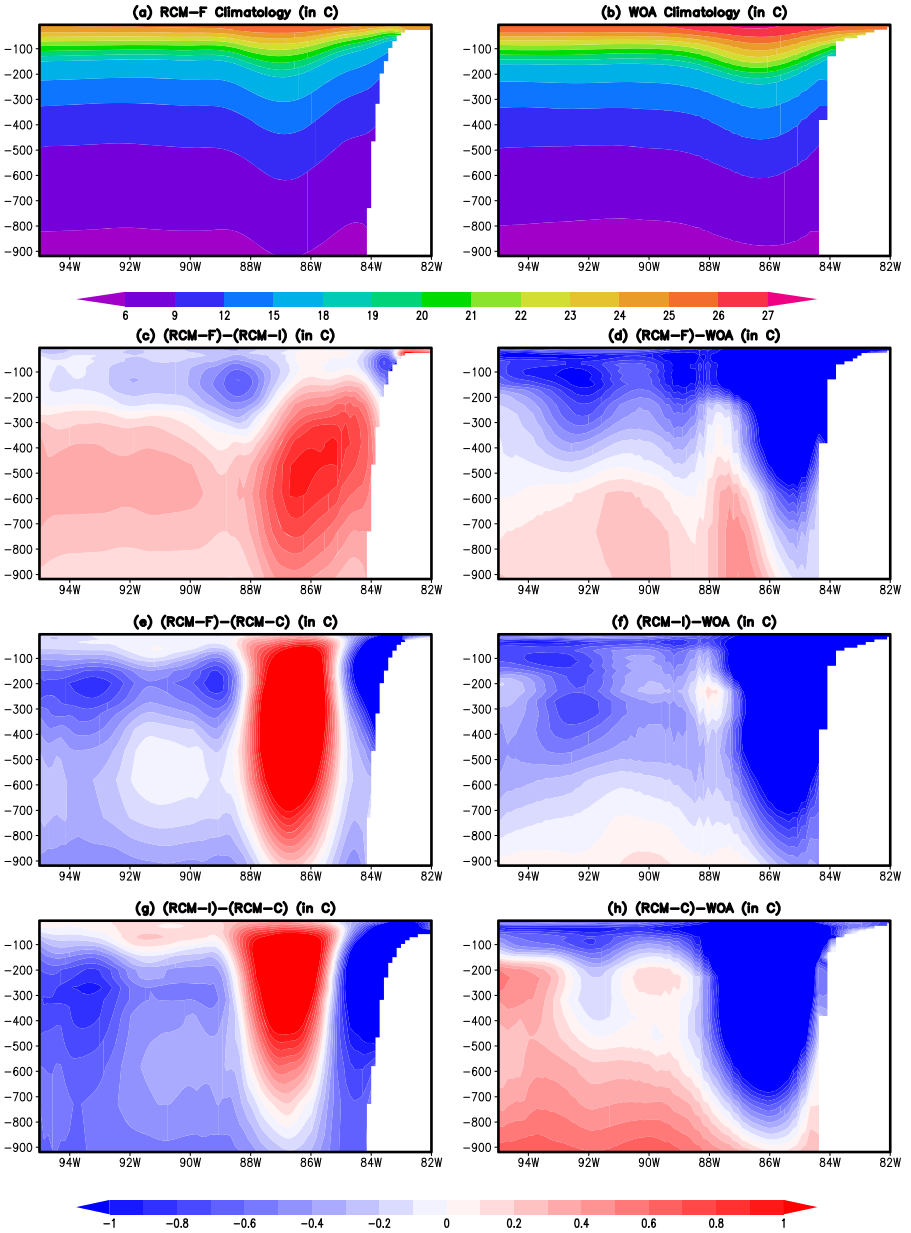


**Fig. 7.** Vertical cross-section of the climatological annual mean temperature (°C) at 25°N (along central GoM) from a) RCM-F and b) WOA. The corresponding difference of RCM-F from c) RCM-I (RCM-F-RCM-I), e) RCM-C (RCM-F-RCM-C) and g) the difference (RCM-I)-(RCM-C). Similarly the corresponding systematic errors from d) RCM-F, f) RCM-I and h) RCM-C.

that the relative warming of RCM-F compared to RCM-I and RCM-C in the Loop Current flow is rather large. However, the temperatures in RCM-F in the first 200 m from the surface are cooler to the west of the Loop Current when compared to both WOA (Fig. 7d) and the other two model simulations (Fig. 7e and g). Interestingly, below 200 m RCM-F is significantly warmer than RCM-I (Fig. 7c) but it is still cooler than RCM-C (Fig. 7e). In addition, the warming in the western GoM (west of 88W) in RCM-I relative to RCM-C (Fig. 7g) is rather shallow near the surface of the ocean. Overall, the systematic errors of RCM-I in this cross section is less than in the other two simulations.

### 5.2. Atmospheric fluxes

As seen in Fig. 8a, the annual mean climatological atmospheric net heat flux in RCM-F is largely positive in the AWP region (south of around 23°N). A positive (negative) net heat flux in this case would mean that the heat flux is directed downward (upward) to (from) the ocean surface. Therefore, in RCM-F there is more net heat flux entering the ocean surface from the

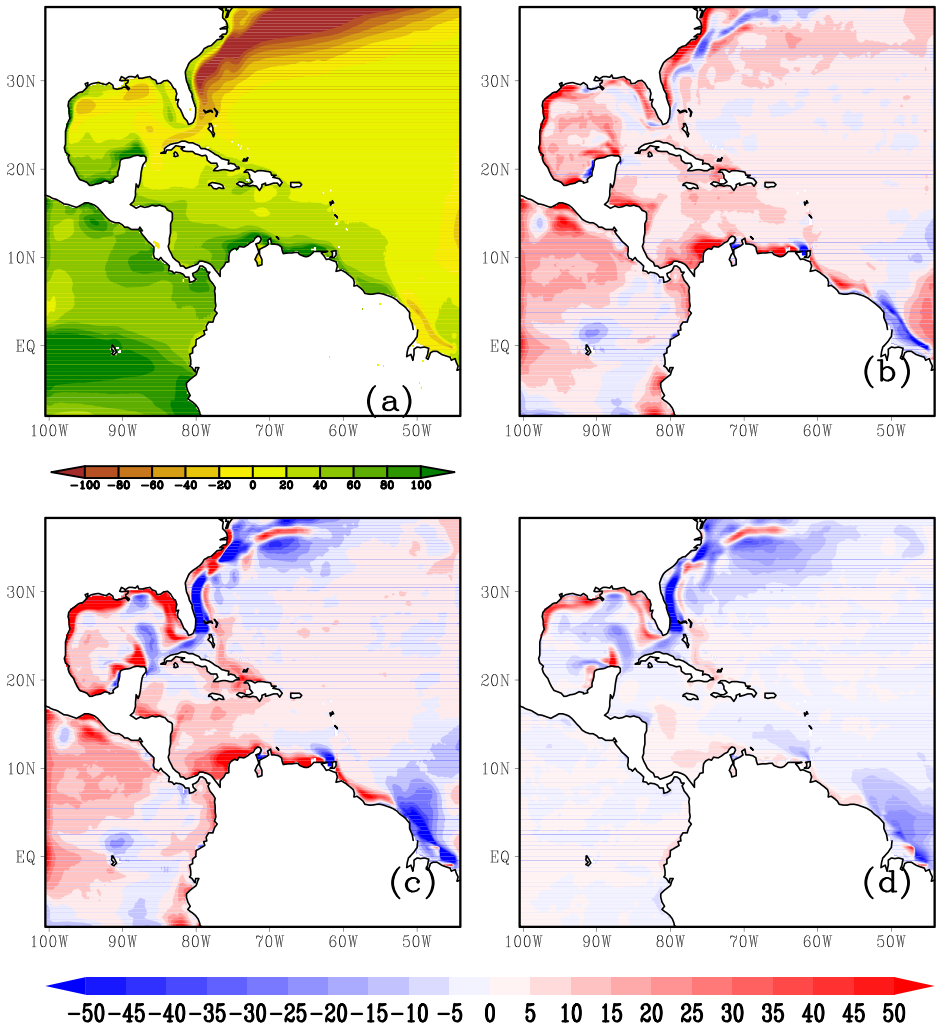


**Fig. 8.** a) The net heat climatological annual mean atmospheric flux from the RCM-F simulation and the corresponding difference with b) RCM-I and c) RCM-C simulations. d) The net het climatological annual mean atmospheric flux difference between RCM-I and RCM-C. The units are in W $m^{-2}$.

atmosphere in the IAS and over western tropical Atlantic Ocean relative to RCM-I (Fig. 8b) and RCM-C (Fig. 8c). Despite this excess heat flux entering the ocean surface (Fig. 8b), RCM-F displays a more severe cold bias over the western GoM and in the Caribbean Sea as compared to RCM-I (Fig. 5g). On the other hand, RCM-I has less heat flux going into the ocean over the central GoM, Bay of Campeche, northern Caribbean Sea, and the northwestern subtropical Atlantic Ocean relative to RCM-F (Fig. 8b) and RCM-C (Fig. 8d). Yet over these regions the SST is warmer in RCM-I relative to both RCM-F (Fig. 5g) or RCM-C (Fig. 5i). Therefore, these contrarian differences in atmospheric fluxes between the model integrations are clearly insufficient to explain the differences in SST between the model simulations (Fig. 5).

### 5.3. Upper ocean heat content

Fig. 9a–c show the annual mean climatological depth of the 20 °C (a proxy for the upper ocean heat content) from the RCM-F, RCM-I, and RCM-C integration respectively. The corresponding bias in RCM-F, RCM-I, and RCM-C are illustrated in Fig. 9d–f respectively, while the differences between RCM simulations are shown in Fig. 9g–i. In relation to the SODA ocean reanalysis, all three RCM simulations underestimate the heat content in the GoM, the Caribbean Sea, and parts of the western tropical Atlantic Ocean (Fig. 9d–f). These errors are most exacerbated in RCM-F over the western GoM and the western Caribbean Sea (Fig. 9g–i). We observe a relative deepening of the 20 °C isotherm in RCM-F over the tropical and subtropical western Atlantic Ocean relative to RCM-I and RCM-C (Fig. 9g and h), however RCM-I displays the largest improvement in this bias over the IAS relative to the other two RCM simulations.

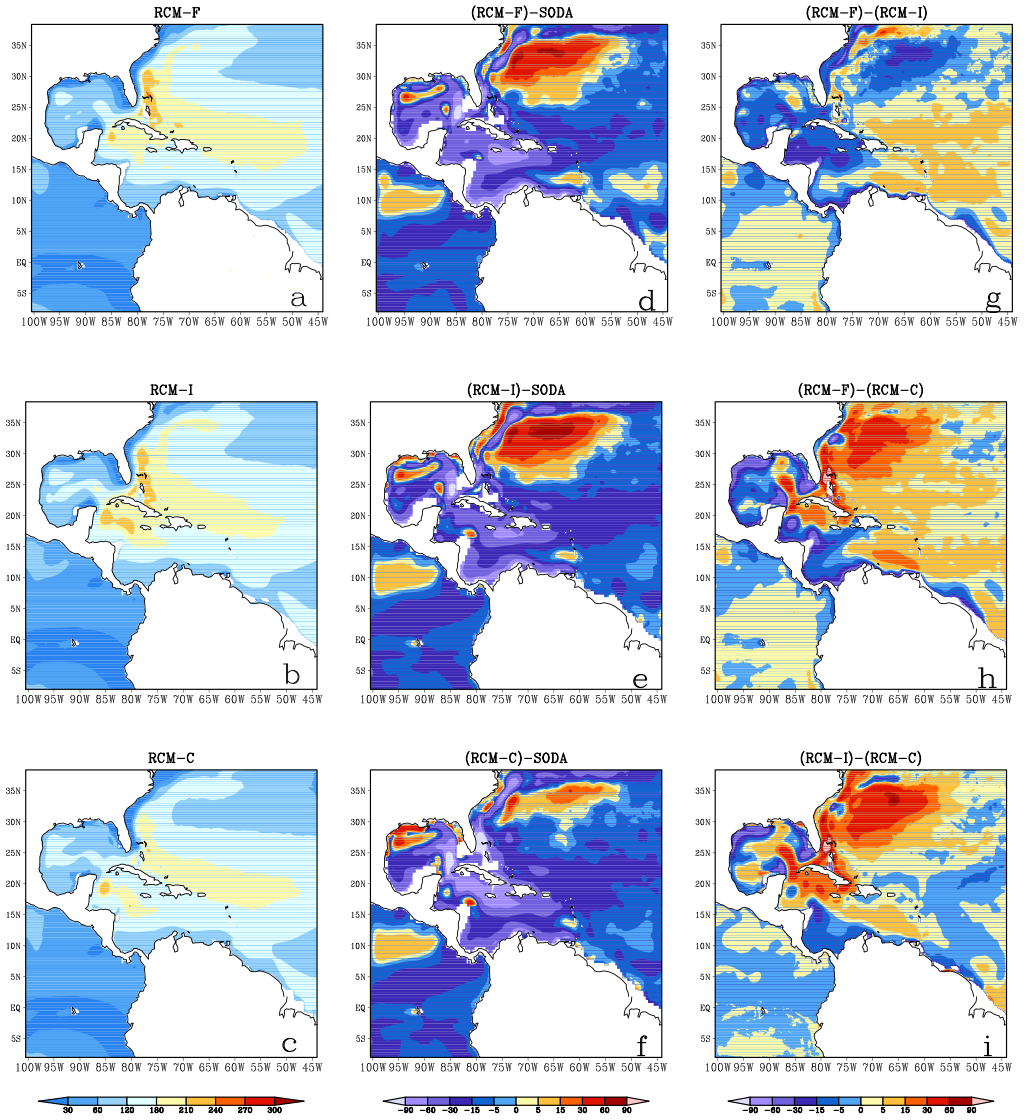


**Fig. 9.** Same as Fig. 5 but for the annual mean climatological depth of the 20 °C isotherm. SODA ocean reanalysis is used for validation. The units are in m.

### 5.4. Ocean currents

The climatological annual mean surface ocean currents from RCM-F, RCM-I, and RCM-C are shown in Fig. 10a–c respectively. The biases of these currents in the RCM simulations indicate that the surface westward Caribbean currents are stronger than the observations (Fig. 10d–f). But unlike the other two simulations, RCM-C has a considerably weaker surface Loop Current and surface flow along the Florida Current (Fig. 10f–i). RCM-F displays the strongest surface Loop Current of all three RCM simulations, although its difference from RCM-I is comparably far smaller (Fig. 10g) than that from RCM-C (Fig. 10h). Furthermore, the northward extension of the Loop Current is extremely weak in RCM-C while the meridional current of the Florida Current is shifted further eastward in RCM-C relative to the observations and the other RCM simulations.

Fig. 11a–d show the cross section of the climatological annual mean flow through the YC in SODA ocean reanalysis, RCM-F, RCM-I, and RCM-C integrations respectively. The differences in the bathymetry of the YC between the SODA, RCM-F and RCM-C simulations are quite apparent in the figure, although the differences of the flow through YC and the bathymetry between RCM-F (Fig. 11b) and RCM-I (Fig. 11c) are comparably much smaller. In RCM-C (Fig. 11d) the channel depth is appreciably shallower than in the RCM-F, RCM-I and SODA ocean reanalysis. Therefore the meridional flow through the channel is also significantly different in RCM-C relative to RCM-F and SODA. For example, the meridional current through the YC shows the asymmetric maximum northward flow on the westward side of the channel in SODA ocean reanalysis (Fig. 11a) and RCM-F simulation (Fig. 11b). This asymmetry in the flow near the surface through the YC is progressively reduced in RCM-I (Figs. 11c and e) and RCM-C (Fig. 11d, f, and g).

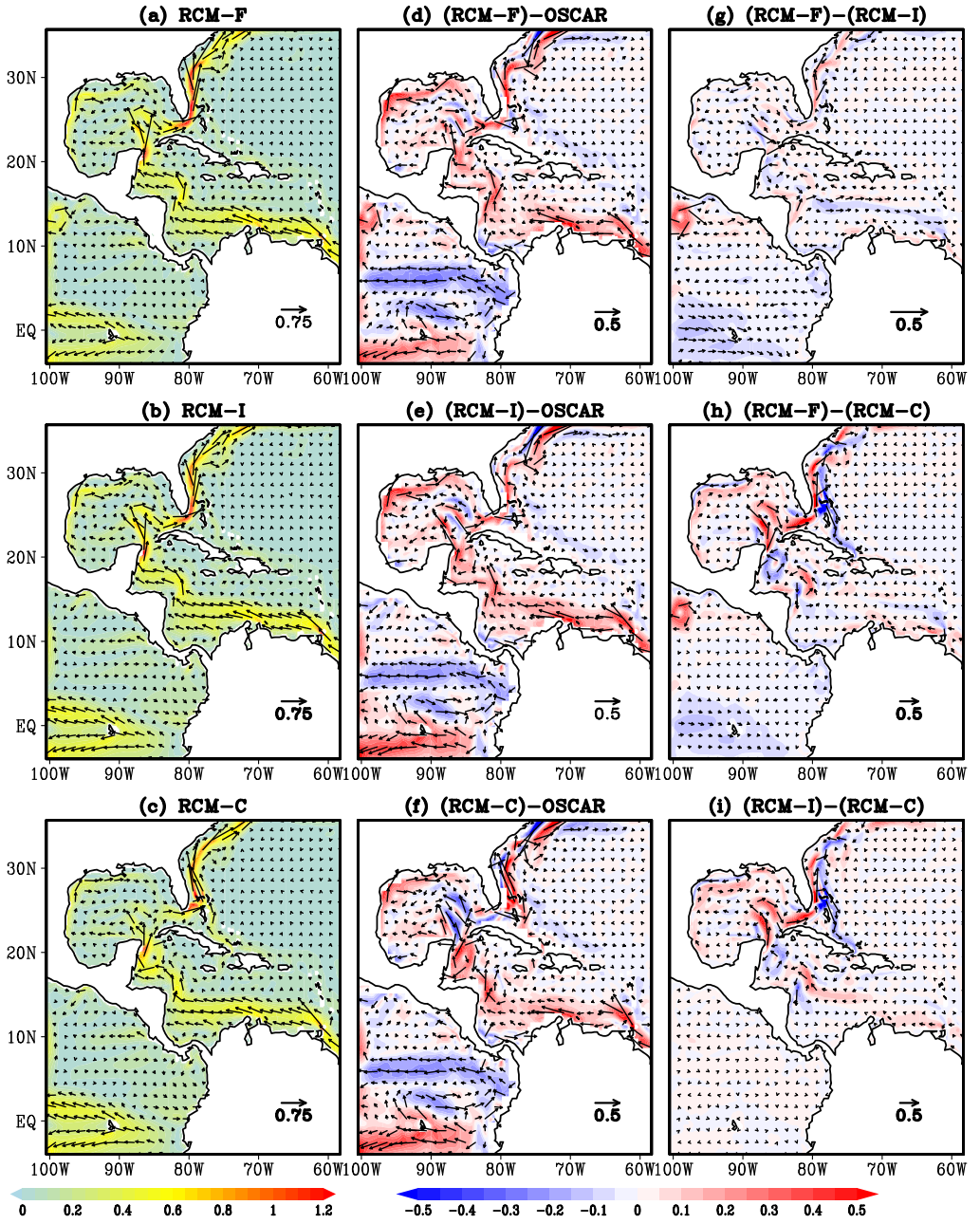


**Fig. 10.** Same as Fig. 5 but for surface ocean currents and OSCAR (Bonjean and Lagerloef, 2002) is used for validation. The units are in m/s.

The maximum surface meridional speed in the RSM-F is approximately 0.7 $ms^{-1}$ (Fig. 11b), which is less than the maximum in SODA ocean reanalysis that display a maximum of around 1.1 $ms^{-1}$ (Fig. 11a). The RCM-F (Fig. 11b) and RCM-I (Fig. 11c) integrations also produce counter currents on both the Yucatan and Cuban sides of the channel, below around 400 m as is mentioned in the observational study of Candela et al. (2003). The SODA reanalysis, however, shows the counter current across the channel at around 1000 m below the surface, which is contrary to the observations made by Candela et al. (2003), who asserted that there is a persistent weak flow toward the GoM in the central deepest part of the channel surrounded by the counter currents on either side. In Fig. 11a, we also note a surface counter current identified in Candela et al. (2003) as the Cuban counter current, which extends to 200 m in depth. The RCM-F (Fig. 11b) and RCM-I (Fig. 11c) integrations reveal this feature, although far more confined to the eastern edge of the channel. However the RCM-C integration does not show this feature of the surface Cuban counter current (Fig. 11d).

The monthly mean volume flux and heat flux through the YC from the three RCM simulations and SODA ocean reanalysis is shown in Fig. 12a and b respectively. We clearly observe from the figures that RCM-C (RCM-F) has the least (largest) vol-

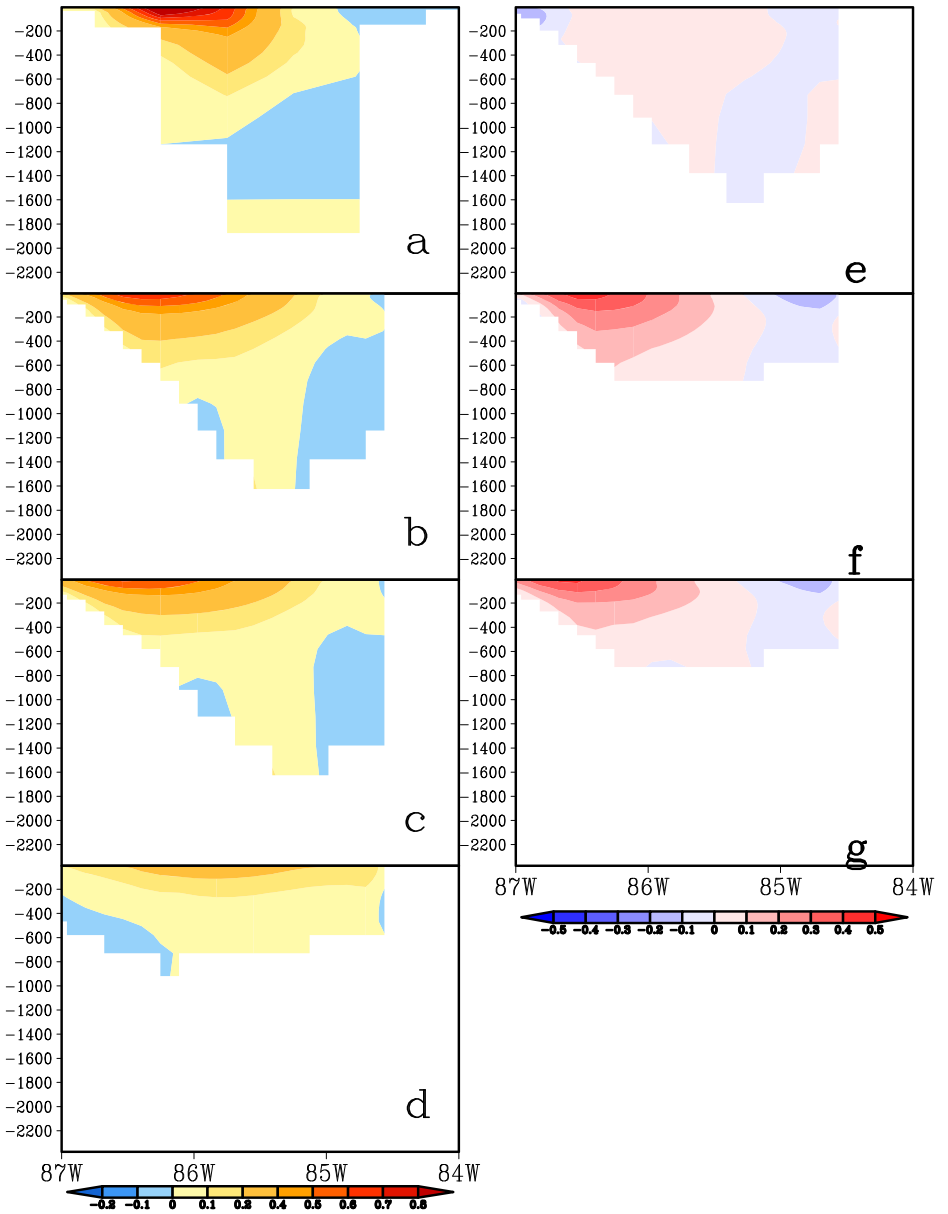


**Fig. 11.** Vertical cross section of the meridional flow ($ms^{-1}$) through the Yucatan Channel from a) SODA ocean reanalysis, b) RCM-F, c) RCM-I, and d) RCM-C integrations. The corresponding differences ($ms^{-1}$) between e) (RCM-F)-(RCM-I), f))(RCM-F)-(RCM-C), and g))(RCM-I)-(RCM-C) are also shown.

ume and heat fluxes through the YC, with RCM-I displaying the closest match to estimates from the SODA ocean reanalysis. In comparison to the corresponding estimates from the global models in Figs. 1 and 2, the bias in RCM-C (of underestimation of flow through YC) resembles the corresponding bias in GFDL-ESM2G while the bias in RCM-F (of overestimation) is closest to the corresponding bias in CCSM4. It should also be noted that there is considerable variability in the estimates of these fluxes through YC from SODA ocean reanalysis from Figs. 1 and 2–Fig. 12, which was computed over different time periods. This is not surprising given similar disparity from in situ observations of the flow through the channel over different periods (Athie et al., 2015). Furthermore, it should be taken into account that all three RCM simulations overestimate the standard deviation of the volume and heat flux through the YC relative to SODA ocean reanalysis and the global models.

Similarly, we also computed the annual mean climatology of the vertically integrated heat transport (HT) vectors from all three RCM simulations in Fig. 13. This HT is computed as:

$$\vec{HT} = c_p \int_{bot}^{surf} \rho \vec{V} \theta dz \tag{1}$$

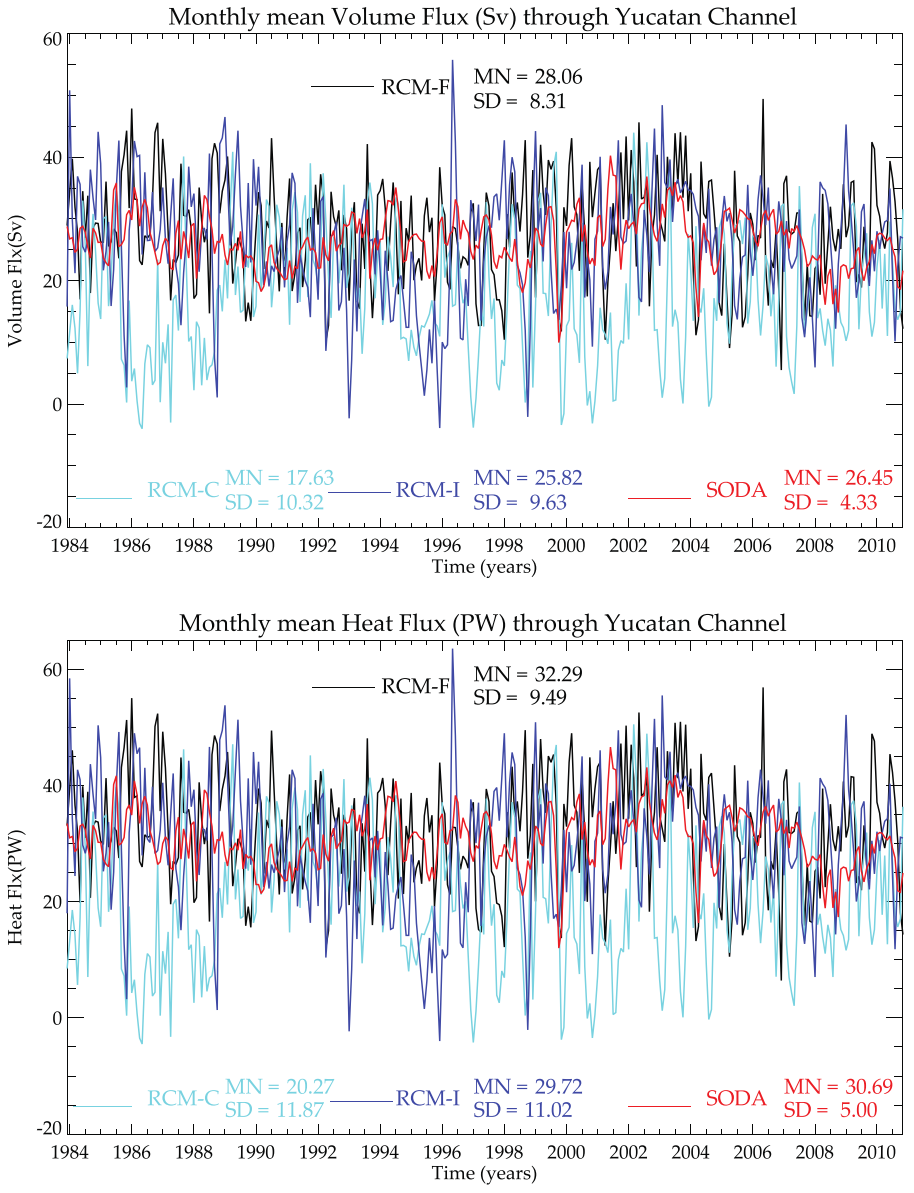


**Fig. 12.** The monthly mean a) volume (in Sv) and b) heat flux (in PW) from the three RCM integrations and the SODA ocean reanalysis.

In Fig. 13a–c, the heat transport by the warm Caribbean Current and the Loop Current, the Gulf Stream, and the return flow of the deep western boundary current is evident in all three RCM simulations. The heat transport by the upper ocean currents are reasonably well represented in the RCM-F and RCM-I simulations. But the heat transport by the return flow of the deep western boundary current is much stronger in the RCM simulations than SODA ocean reanalysis (Fig. 13d–f). The heat transport by the Loop Current in RCM-F and RCM-I also display a stronger northeastward tilt north of the YC as compared to SODA, while the RCM-C simulation displays a very weak heat transport through the YC (Fig. 13f). The differences in the heat transport in the AWP region between RCM-F and RCM-I are much smaller (Fig. 13g) relative to their corresponding difference from RCM-C (Fig. 13h and i). The RCM-C also has minimal heat transport through the Windward and Mona passages relative to the other two RCM simulations and the SODA ocean reanalysis.

### *5.5. Interannual variability*

The contemporaneous correlation between the sea surface height and the volume flux through the YC is shown in Fig. 14. In the SODA ocean reanalysis (Fig. 11a), we observe that the heat content in northern Caribbean Sea around Cuba and the Bahamas increases when the flow through the YC is stronger. However, stronger flow through the YC is also associated with

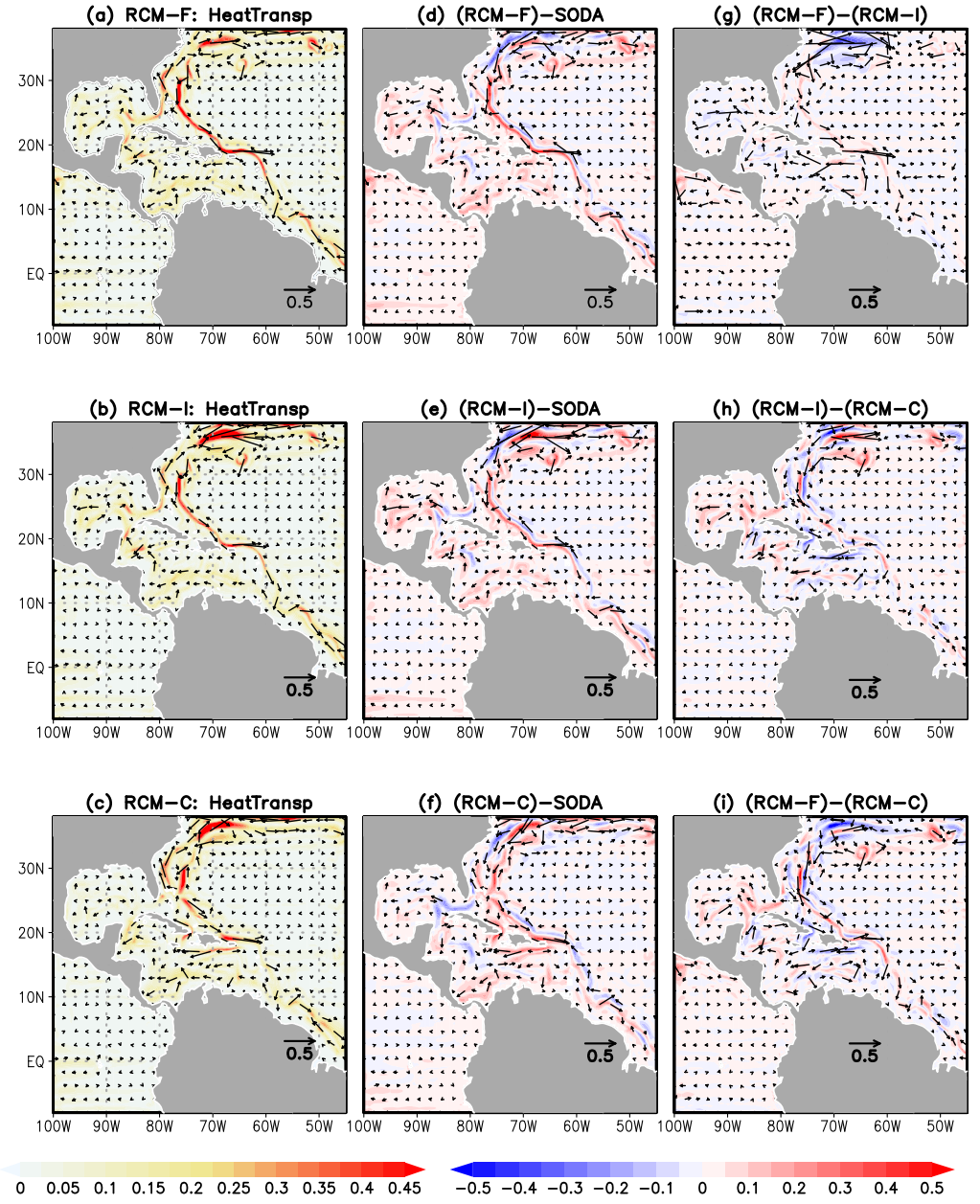


**Fig. 13.** Same as Fig. 5 but for ocean heat transport vector (Eq. (1)). We use the SODA ocean reanalysis for validation. The units are TerraWatt [TW] ($=1 \times 10^{12}$ W).

a reduction in the heat content around the GoM coast along the Florida Current, as well as the western and southern coast of the Caribbean Sea (Fig. 14a). These features are reasonably well captured by the RCM-I (Fig. 14c) with subtle differences (e.g. over northwestern tropical Atlantic Ocean, the Caribbean coast of Central America, and northern South America). On the other hand, the RCM-F integration (Fig. 14b) is comparable to RCM-I but the relationship along the GoM coasts and the Caribbean Sea coast along Central America and northern South America is weak and even contrary to the SODA ocean reanalysis and RCM-I. But RCM-C correlations (Fig. 14d) show a far worse fidelity with respect to the SODA ocean reanalysis both in the magnitude and spatial extent of the correlations.

In fact, the correlations displayed in Fig. 14a and c are similar to those obtained in Lin et al. (2009), which were acquired from a model integration data over a much shorter period of time using a very high resolution (1/6°) ocean model. Their study showed that the transport through the YC is a minimum when the Loop Current intrudes strongly into the GoM. Furthermore, they suggested that variations of the sea surface height around Cuba is a result of a “compensation effect” in

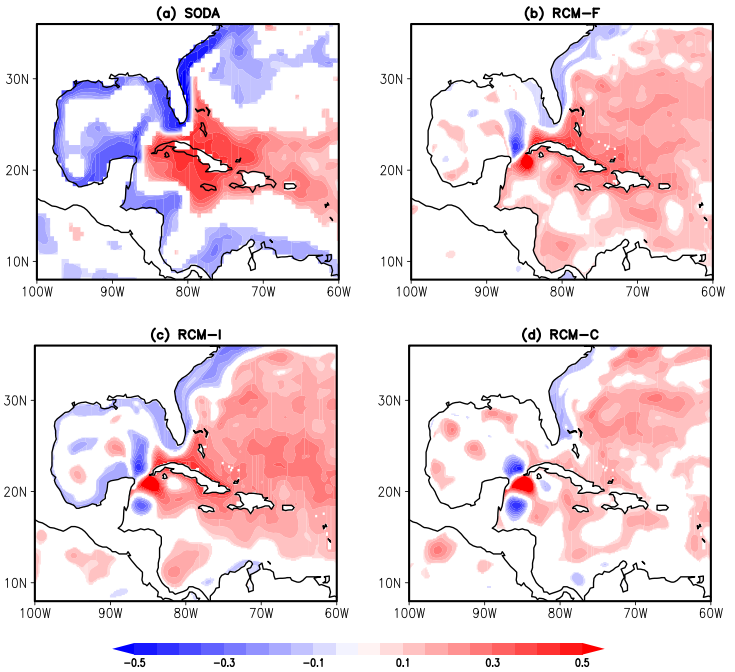


**Fig. 14.** The contemporaneous correlations of the flow through the Yucatan Channel with sea surface height anomalies from a) SODA, b) RCM-F, c) RCM-I and d) RCM-C integrations. Only significant values at 10% significance level according to *t*-test are plotted.

which the variability of the flow through the YC is partially compensated by the variability of the flow around Cuba (through the Old Bahama Channel).

## 6. Discussion

In this section we will relate the bias in the two 20th century simulations from the suite of CMIP5 models (GFDL-ESM2G and CCSM4) analyzed earlier to the results from our RCM integrations. Although GFDL-ESM2G grossly underestimated the ocean transport through the YC, the SST bias was similar to that exhibited by CCSM4, which grossly overestimated the flow through the YC. It may however be noted that the severity of the cold bias in GFDL-ESM2G is more acute. We obtain a similar result from the three RCM integrations analyzed in this study. RCM-F overestimates the transport through the YC and yet it exhibits a cold SST bias over the IAS, which is comparable to RCM-C that displays a gross underestimation of the flow through the YC. Our third RCM-I integration ameliorates some of this cold SST bias relative to RCM-F and RCM-C. The RCM-I simulation shows the flow through the YC is closest to the observed estimates (Athie et al., 2015) and the SODA ocean reanalysis as compared to the other two RCM simulations (Fig. 12).

The increased flow through the YC has a significant impact on raising the upper ocean heat content and SST in the tropical and subtropical western Atlantic Ocean (Figs. 9i, 5a and b). Therefore RCM-F, which has the strongest flow through the YC, displays SST warming over a considerable region across tropical-subtropical western Atlantic Ocean relative to both RCM-I (Fig. 5g) and RCM-C (Fig. 5h). This is also associated with considerable weakening of the atmospheric surface tropical easterlies across the IAS in RCM-F (especially over the GoM and the Caribbean Sea; Fig. 15). In a related modeling study Chang and Oey (2010a) suggested that heat is transported to the western part of the GoM primarily by wind-induced westward shelf currents. These currents converge in the western GoM (along the TAVE and LATEX shelves) where they downwell and spread heat to the interior of the ocean. As noted in Fig. 14a–c, the negative correlations of the sea surface height variations in the Bay of Campeche and along the TAVE, LATEX and Florida shelves with the transport through the YC is consistent with this feature. In fact, similar correlations are also observed south of the YC, along the eastern continental shelf of Mexico in Fig. 14a and c. In RCM-C (Fig. 14d), where the flow through the YC is very weak, the associated sea surface height variations along the shelf in the western GoM and Caribbean Sea are weak and contrary to the SODA ocean reanalysis. The absence of negative correlations in RCM-F along the TAVE and LATEX shelves and along the western Caribbean coast is a result of significant weakening of the shelf currents from the corresponding weakening of the atmospheric tropical easterlies. This weakening of the low-level atmospheric easterlies results from the coupled air-sea feedback mechanism. One of the air-sea coupled feedback mechanisms is preferentially fostered in the boreal summer season by a Gill-type atmospheric response to off equatorial forcing of AWP induced heating (Wang and Enfield, 2001; Wang et al., 2007, 2008a, 2008b; Lee et al., 2009). These studies clearly demonstrate that atmospheric latent heating induced by the warm SSTs of the seasonal AWP induce both baroclinic and barotropic responses that have a tendency to weaken the easterly Atlantic trade winds.

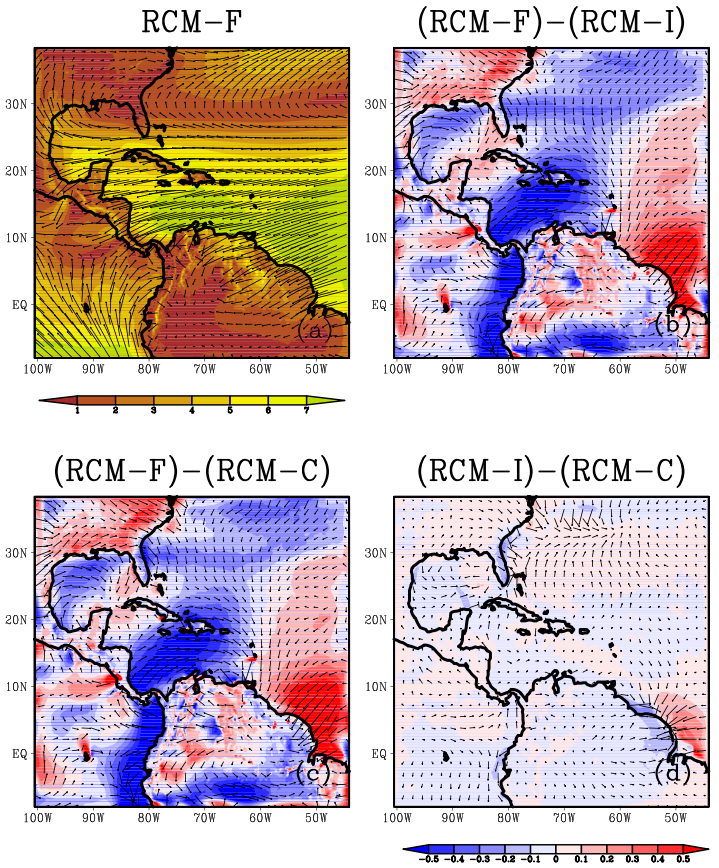


**Fig. 15.** a) Annual mean climatology of the 1000 hPa winds from RCM-F run and its corresponding difference from b) RCM-I, c) RCM-C. Similarly, the climatological annual mean difference of the 1000 hPa winds between RCM-I and RCM-C integrations.

In addition, the coupled feedback of wind-induced evaporation can also affect the trade winds and SST in the tropical-subtropical Atlantic (Moura and Shukla 1981; Hastenrath and Greischar 1993; Chang et al., 1997). This mechanism involves changes in the atmospheric boundary layer pressure gradient induced by changes in SST (e.g. from seasonal evolution or variability) affecting the overlying atmospheric surface winds (Lindzen and Nigam, 1987) that feeds back to SST through wind induced evaporation (Chang et al., 1997). Furthermore, Tanimoto and Xie (2002) suggested cloud feedback on SST that manifest in coupled feedback in the tropical and subtropical Atlantic Ocean.

In Fig. 16 we show the climatological cross-section of zonal heat flux (Eq. (2) across 90 °W following Chang and Oey (2010a) from the SODA and three RCM simulations.

$$HF = c_p \int_{bot}^{surf} \rho u \theta dz \tag{2}$$

where u is the zonal current. In the SODA ocean reanalysis heat is transported westward into the western GoM both on the southern and northern shelf, while in the middle of the basin heat is transported eastward as described in Chang and Oey, 2010b. However, in the three RCM simulations heat is transported westward only in the southern shelf while heat is transported eastward in the northern shelf and in the upper ocean in middle of the basin. It is also quite apparent that the eastward flow of heat to western GoM is strongest in RCM-I (Fig. 16c) and least in RCM-F (Fig. 16b). Chang and Oey (2010a) indicated from their idealized modeling studies that wind-induced currents along the northern and southern shelves of the GoM play an important role in the westward heat redistribution, which is also reaffirmed from the three RCM simulations conducted in this study. The eastward heat transport in the northern shelf is part of the Gulf-scale anticyclonic gyre that dominates over the shelf currents under weak wind situation (Chang and Oey, 2010b). Chang and Oey (2010a) further suggested that these shelf currents induce downwelling as they flow off the shelf edge after converging in the western coast, thereby transporting heat eastward in the central GoM as is seen in Fig. 16a–d.

This study clearly shows that overcompensation of the flow through the YC (e.g. in RCM-F) can result in SST bias, at least over the western GoM and even over western Caribbean Sea, that resemble the SST bias from model simulations that under-compensate the flow through the YC (e.g. RCM-C). Notably, 1000 hPa climatological winds in the 20th century simulations

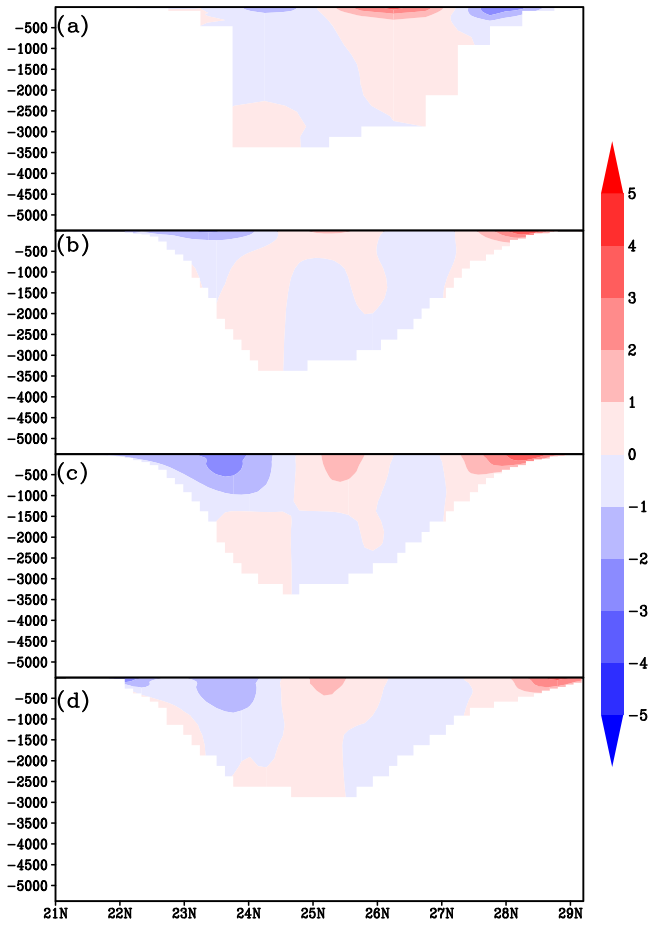


**Fig. 16.** Annual mean climatological heat flux across 90°W from a) SODA, b) RCM-F, c) RCM-I, and d) RCM-C. The units are ($10^8$ W m$^{-2}$).

of CCSM4 and GFDL-ESM2G show similar differences as RCM-F and RCM-C, respectively, suggesting a similar mechanism for the SST bias in the western part of IAS (not shown). That said, it should also be noted that all three RCM integrations display a cold SST bias in the IAS despite their varied representation of the IAS ocean circulation, which would suggest that other sources of error (e.g. atmospheric fluxes; remote teleconnections) are likely in play. This is further elaborated by verifying the atmospheric fluxes in the simulation (Fig. 17).

The observed annual mean climatological atmospheric fluxes suggest that in the northern parts of the AWP region there is a net upwelling atmospheric flux while in the southern Caribbean Sea and southwestern GoM there is a net downwelling atmospheric flux (Fig. 17a). The COREII analysis suggests that the upwelling longwave fluxes (Fig. 17b) and the enthalpy (sensible and latent heat) fluxes (Fig. 17d) compensate for the downwelling shortwave flux (Fig. 17c) in the AWP region. The corresponding systematic errors of the fluxes in RCM-F (Fig. 17e–h), RCM-I (Fig. 17i–l), and RCM-C (Fig. 17m–p) are comparable. Furthermore, it seen that these model simulations overestimate the downwelling shortwave flux significantly, which is over compensated by the overestimation of the upwelling longwave flux and enthalpy fluxes to result in a net heat flux that is upwelling in the AWP region. It is interesting to note that despite the decrease in the easterly trades in RCM-F the upwelling enthalpy fluxes are still large, which stems from a dry bias in the boundary layer (not shown). This dry bias increases the humidity gradient between the surface and the boundary layer thereby raising the enthalpy fluxes. The dry bias in the boundary layer also contributes to increased upward longwave flux as well as a lower shallow cloud fraction relative to corresponding the observed cloud fraction (Rossow et al., 1996; not shown), which results in higher downwelling shortwave flux in all three model simulations. Furthermore, it seems clear that the bias in the net heat flux from the model simulations is far larger over the open oceans than the inter-model differences, which are significantly large in the coastal and over broad (shallower) continental shelf regions (see Fig. 8).

## 7. Summary and conclusions

In this study we conduct three multi-decadal integrations (for a duration of 32 years) with a relatively high resolution (15 km) regional coupled ocean-atmosphere model (RCM) centered over the IAS. These model integrations are conducted

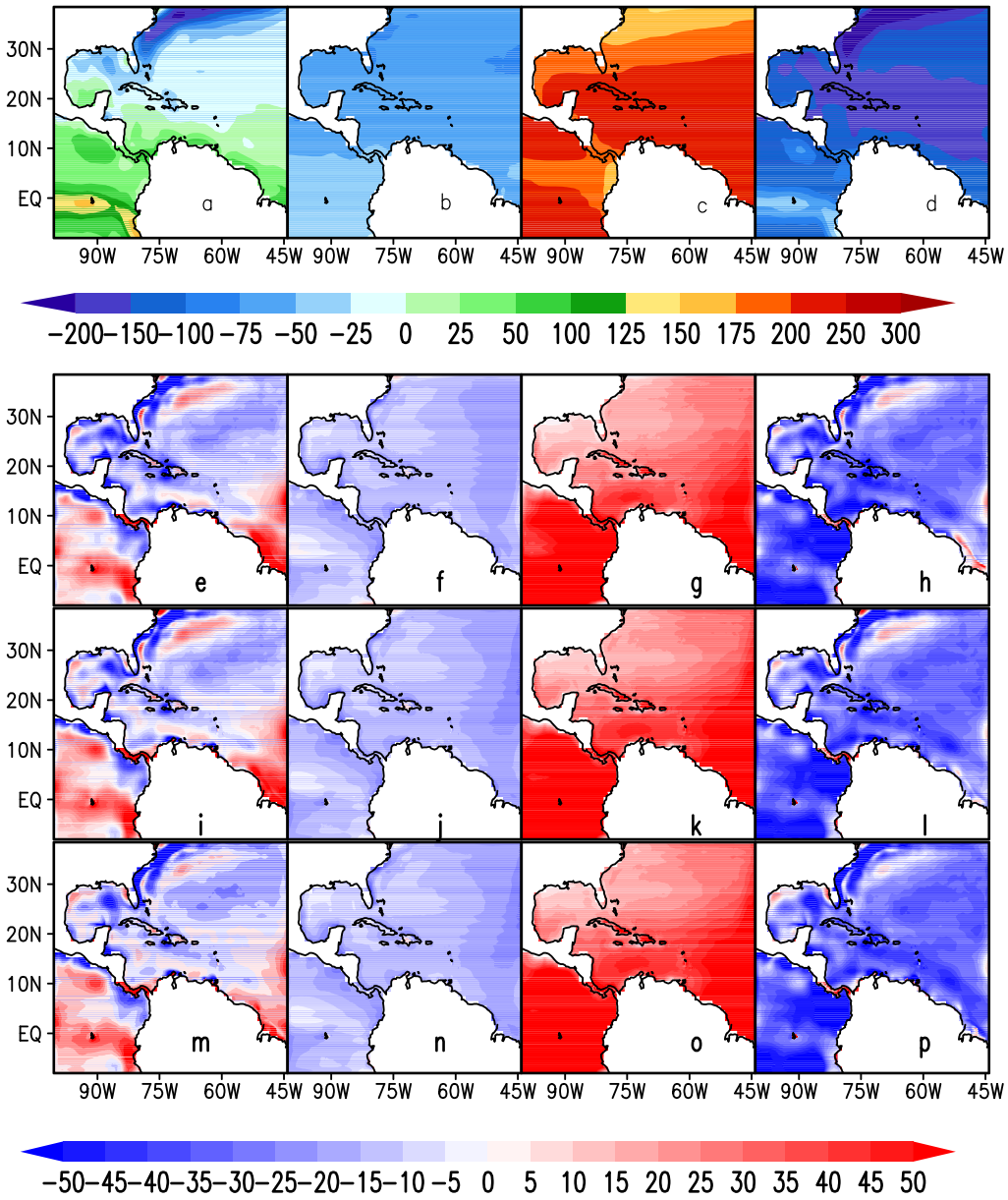


**Fig. 17.** The annual mean climatological a) net heat flux, b) upwelling longwave flux, c) downwelling shortwave flux, and d) enthalpy (sensible and latent) fluxes from COREII. Positive (negative) sign of fluxes indicate into (out of) the ocean surface. The corresponding systematic errors of the fluxes from RCM-F (e–h), RCM-I (i–l), and RCM-C (m–p). The units are in $W m^{-2}$.

with the same numerical model at identical spatial resolution and with the same lateral boundary conditions for the atmosphere and the ocean. However, the important difference in these integrations is that they are prescribed uniquely different bathymetries. As a result, some of the topographical features including the depth of the YC, Florida Straits, and the slope of the continental shelves were different in these RCM integrations. In terrain following models such as ROMS, smoothing of the bathymetry is customary to avoid large errors in the computation of the horizontal pressure gradient in the presence of steep gradient in bathymetry. An important part of this study is understanding the potential sources of error in simulating the climate of a region such as the IAS, which displays complex bathymetry and hosts a very large and very warm pool of water in part of the year that elicits strong atmospheric response.

These model experiments highlight the importance of ocean circulation in the maintenance of the heat content and SST structure in the IAS region. Our results suggest that differences in bathymetry, primarily those that affect the flow through the YC, can have a significant impact on the ocean circulation and temperature in the IAS region. However, a sobering and a counter-intuitive result is that a more realistic bathymetry does not uniformly improve the simulation over the IAS owing

to other sources of model errors. It is noted that all model simulations of the study systematically underestimate the net heat atmospheric flux into the ocean.

This study draws attention to the general surface manifestation of colder SSTs and the underestimation of upper ocean heat content generated by the smoother bathymetry over most parts of the IAS, similar to the bias displayed by majority of the general circulation models. In the case of the RSM-ROMS integration with the smoother bathymetry (RCM-C), we show that this surface manifestation of a colder SST is more acute than in RCM-I or RCM-F over the southern limb of the Gulf Stream, followed then by that over the GoM, the northern Caribbean Sea, and parts of tropical and subtropical western Atlantic Ocean. There are, however, regions over the southern Caribbean Sea, along the LATEX shelf, and along the northeast GoM coast where the RCM-C is warmer than RCM-F.

As a result of the shallower depth of the YC in the RCM-C there is a clear reduction in the mean meridional flow through the Channel. Furthermore, the Windward Passage in RCM-C exhibits direction of heat transport contrary to either RCM-F or SODA reanalysis. Both of these factors affect the heat transport by the Gulf Stream in the RCM-C resulting in larger biases of SST and heat content in the IAS and western tropical and subtropical Atlantic Ocean.

The flow through the YC clearly impacts the heat content locally and remotely in a large section of the IAS region by affecting the heat transport by the prevailing upper ocean currents in the region. But RCM-C significantly underestimates the flow through the YC and RCM-F overestimates the flow through the YC. Yet, both exhibit a cold SST bias that is similar to the bias displayed by GFDL-ESM2G and CCSM4 20th century simulations over the IAS. We find that the warming of the upper ocean in the western tropical and sub-tropical Atlantic Ocean in RCM-F from the increased Loop Current circulation results in significant weakening of the overlying atmospheric easterlies. This, in turn, weakens the wind-induced shelf currents in the western GoM and the Caribbean Sea, thus exacerbating the SST bias in RCM-F relative to RCM-I and RCM-C. Notably, although alike in RCM-C and RCM-F, the cause of SST bias is quite different — the former is a consequence of a weakened Loop Current while the latter results from a coupled ocean-atmosphere response to a stronger Loop Current. The former (RCM-C) would benefit from an improved bathymetry while the latter (RCM-F) would likely improve from better coupled response of the atmosphere to SST anomalies in the IAS. And all three RCM simulations would benefit from improved parameterization of the atmospheric fluxes as they uniformly overestimate the downwelling shortwave flux, upwelling longwave flux, and the enthalpy fluxes. In the meantime, despite its slightly inferior bathymetry to RCM-F, RCM-I shows a comparatively smaller SST bias in the IAS through a likely compensation of errors in the ocean and atmospheric components of the RCM.

## Acknowledgements

The authors would like to thank Ms. Tracy Ippolito of the Center for Ocean-Atmospheric Studies, Florida State University for the editorial assistance. This work was supported by grants from NOAA (NA12OAR4310078, NA11OAR4310110) and USGSG13AC00408. The supercomputing facility provided by XSEDE under grant number ATM10010 was used to complete the model integrations used in this study.

## References

Alpert, J.C., Kanamitsu, M., Caplan, P.M., Sela, J.G., White, G., Kalnay, E. 1988. Mountain induced gravity wave drag parameterization in the NMC medium-range model. Preprints, Eighth conference on Numerical Weather Prediction, American Meteorological Soc., Baltimore, MD, pp. 726–733.

Athie, G., Sheinbaum, J., Leben, R., Ochoa, J., Shannon, M.R., Candela, J., 2015. Interannual variability in the Yucatan Channel flow. Geophys. Res. Lett. 42, 1496–1503, http://dx.doi.org/10.1002/2014GL062674.

Bonjean, F., Lagerloef, G.S.E., 2002. Diagnostic model and analysis of the surface currents in the tropical pacific ocean. J. Phys. Oceanogr. 32, 2938–2954, http://dx.doi.org/10.1175/1520-0485(2002)032<2938:DMAAOT>2.0.CO;2.

Bosart, L.F., Lin, S.C., 1984. A diagnostic analysis of the Presidents' Day storm of February 1979. Mon. Wea. Rev. 112, 2148–2177, http://dx.doi.org/10.1175/1520-0493(1984)112<2148:ADAOTP>2.0.CO;2.

Businger, S., Knapp, D.I., Watson, G.F., 1990. Storm following climatology of precipitation associated with winter cyclones originating over the gulf of Mexico. Weather Forecasting 5, 378–403, http://dx.doi.org/10.1175/1520-0434(1990)005<0378:SFCOPA>2.0.CO;2.

Candela, J., Tanahara, S., Crepon, M., Barnier, B., Sheinbaum, J., 2003. Yucatan channel flow: observations versus CLIPPER ATL6 and MERCATOR PAM models. J. Geophys. Res. 108 (C12), 3385–3408, http://dx.doi.org/10.1029/2003jc001961.

Carton, J.A., Giese, B.S., 2008. A reanalysis of ocean climate using simple ocean data assimilation (SODA). Mon. Weather Rev. 136, 2999–3017, http://dx.doi.org/10.1175/2007MWR1978.1.

Chérubin, L.M., Sturges, W., Chassignet, E.P., 2005. Deep flow variability in the vicinity of the Yucatan Straits from a high-resolution MICOM simulation. J. Geophys. Res. 110, C04009, http://dx.doi.org/10.1029/2004JC002280.

Cherubin, L.M., Morel, Y., Chassignet, E.P., 2006. Loop current ring shedding: the formation of cyclones and the effect of topography. J. Phys. Oceanogr 36, 569–591.

Chan, S., Misra, V., 2010. A diagnosis of the 1979–2005 extreme rainfall events in the southeastern United States with isentropic moisture tracing. Mon. Weather Rev. 138, 1172–1185, http://dx.doi.org/10.1175/2009MWR3083.1.

Chang, Y.–L., Oey, L.–Y., 2010a. Why can wind delay the shedding of Loop Current Eddies? J. Phys. Oceanogr. 40 (11), 2481–2495, http://dx.doi.org/10.1175/2010JPO4460.1.

Chang, Y.–L., Oey, L.–Y., 2010b. Eddy and wind forced heat transports in the Gulf of Mexico. J. Phys. Oceanogr. 40 (12), 2727–2742, http://dx.doi.org/10.1175/2010JPO4474.1.

Chang, P., Ji, L., Li, H., 1997. A decadal climate variation in the tropical Atlantic ocean from thermodynamic air-sea interactions. Nature 385, 516–518.

Chou, M.-D., Lee, K.-T., 1996. Parameterizations for the absorption of solar radiation by water vapor and ozone. J. Atmos. Sci. 53, 1203–1208, http://dx.doi.org/10.1175/1520-0469(1996)053<1203:PFTAOS>2.0.CO;2.

Chou, M.-D., Suarez, M.J., 1994. An efficient thermal infrared radiation parameterization for use in general circulation models. Technical report series on global modeling and data assimilation, NASA/TM-1994-104606, 3, pp. 85.

Clement, A.C., Seager, R., Murtugudde, R., 2005. Why are there tropical warm pools? J. Clim. 18, 5294–5311, http://dx.doi.org/10.1175/JCLI3582.1.

Dukhovskoy, D.S., Leben, R.R., Chassignet, E.P., Hall, C., Morey, S.L., Nedbor-Gross, R., 2014. Characterization of the uncertainty in the Gulf of Mexico loop current description using a multi-decadal numerical simulation and altimeter observations. Deep Sea Res. I: Oceanogr. Res. Pap. 100, 140–158, http://dx.doi.org/10.1016/j.dsr.;1;2015.01.005.
Dunne, J.P., John, J.G., Adcroft, A.J., Griffies, S.M., Hallberg, R.W., Shevliakova, E., Stouffer, R.J., Cooke, W., Dunne, K.A., Harrison, M.J., Krasting, J.P., Malyshev, S.L., Milly, P.C.D., Phillipps, P.J., Sentman, L.T., Samuels, B.L., Spelman, M.J., Winton, M., Wittenberg, A.T., Zadeh, N., 2012. GFDL's ESM2 global coupled climate–carbon earth system models. Part I: physical formulation and baseline simulation characteristics. J. Clim. 25, 6646–6665, http://dx.doi.org/10.1175/JCLI-D-11-00560.1.
Ek, M.B., Mitchell, K.E., Lin, Y., Rogers, E., Grunmann, P., Koren, V., Gayno, G., Tarpley, J.D., 2003. Implementation of Noah land surface model advances in the National Centers for Environmental Prediction operational mesoscale Eta model. J. Geophys. Res. 108 (D22), 8851–8866, http://dx.doi.org/10.1029/2002jd003296.
Gent, P.R., Danabasoglu, G., Donner, L.J., Holland, M.M., Hunke, E.C., Jayne, S.R., Lawrence, D.M., Neale, R.B., Rasch, P.J., Vertenstein, M., Worley, P.H., Yang, Z.-L., Zhang, M., 2011. The community climate system model version 4. J. Clim. 24, 4973–4991, http://dx.doi.org/10.1175/2011JCLI4083.1.
Giese, B.S., Ray, S., 2011. El Niño variability in simple ocean data assimilation (SODA), 1871–2008. J. Geophys. Res. 116, C02024, http://dx.doi.org/10.1029/2010JC006695.
Haidvogel, D.B., Arango, H.G., Hedstrom, K., Beckmann, A., Malanotte-Rizzoli, P., Shchepetkin, A.F., 2000. Model evaluation experiments in the North Atlantic Basin: simulations in nonlinear terrain-following coordinates. Dyn. Atmos. Oceans 32, 239–281, http://dx.doi.org/10.1016/S0377-0265(00)00049-X.
Haney, R.L., 1991. On the pressure gradient force over steep topography in sigma coordinate ocean models. J. Phys. Oceanogr. 21, 610–619, http://dx.doi.org/10.1175/1520-0485(1991)021<0610:OTPGFO>2.0.CO;2.
Hastenrath, S., Greischar, L., 1993. Further work on the prediction of northeast Brazil rainfall anomalies. J. Clim. 6, 743–758.
Helber, R.W., Weisberg, R.H., Bonjean, F., Johnson, E.S., Lagerloef, G.S.E., 2007. Satellite-derived surface current divergence in relation to tropical atlantic SST and wind. J. Phys. Oceanogr. 37, 1357–1375, http://dx.doi.org/10.1175/JPO3052.1.
Hong, S.Y., Pan, H.L., 1996. Nonlocal boundary layer vertical diffusion in a medium-range forecast model. Mon. Weather Rev. 124, 2322–2339, http://dx.doi.org/10.1175/1520-0493(1996)124<2322:NBLVDI>2.0.CO;2.
Hurlburt, H.E., Thompson, J.D., 1980. A numerical study of Loop Current intrusions and eddy shedding. J. Phys. Oceanogr. 10, 1611–1651, http://dx.doi.org/10.1175/1520-0485(1980)010<1611:ANSOLC>2.0.CO;2.
Jackett, D.R., McDougall, T.J., Feistel, R., Wright, D.G., Griffies, S.M., 2006. Algorithms for density, potential temperature, conservative temperature, and the freezing temperature of seawater. J. Atmos. Oceanic Technol. 23, 1709–1728, http://dx.doi.org/10.1175/JTECH1946.1.
Jayne, S.R., Marotzke, J., 2002. The oceanic eddy heat transport. J. Phys. Oceaongr. 32, 3328–3345.
Juang, H.-M.H., Kanamitsu, M., 1994. The NMC nested regional spectral model. Mon. Weather Rev. 122, 3–26, http://dx.doi.org/10.1175/1520-0493(1994)122<0003:TNNRSM>2.0.CO;2.
Kanamitsu, M., Ebisuzaki, W., Wollen, J., Yang, S.-K., Hnilo, J.J., Fiorino, M., Potter, G.L., 2002. NCEP-DOE AMIP-II reanalysis. Bull. Amer. Met. Soc. 83, 1631–1643, http://dx.doi.org/10.1175/BAMS-83-11-1631.
Kanamitsu, M., Yoshimura, K., Yhang, Y.-B., Hong, S.-Y., 2010. Errors of interannual variability and multi-decadal trend in dynamical regional climate downscaling and its corrections. J. Geophys. Res. 115, D17115, http://dx.doi.org/10.1029/2009JD013511.
Kozar, M., Misra, V., 2012. Evaluation of twentieth-century atlantic warm pool simulations in historical CMIP5 runs. Clim. Dyn. 41 (9–10), 2375–2391, http://dx.doi.org/10.1007/s00382-012-1604-9.
Large, W.G., Yeager, S.G., 2009. The global climatology of an interannually varying air–sea flux data set. Clim. Dyn. 33, 341–364, http://dx.doi.org/10.1007/s00382-008-0441-3.
Large, W.G., McWilliams, J.C., Doney, S.C., 1994. Oceanic vertical mixing: a review and a model with a nonlocal boundary layer parameterization. Rev. Geophys. 32, 363–403, http://dx.doi.org/10.1029/94RG01872.
Leben, R.R., 2005. In: Sturges, W., Lugo-Fernandes, A. (Eds.), Altimetry-Derived Loop Current Metrics, in Circulation of the Gulf of Mexico: Observations and Models, Geophys. Monogr. Ser., vol. 161. AGU, Washington, D. C, pp. 181–201.
Lee, S.-K., Enfield, D.B., Wang, C., 2005. Ocean general circulation model sensitivity experiments on the annual cycle of Western Hemisphere Warm Pool. J. Geophys. Res. 110, C09004, http://dx.doi.org/10.1029/2004JC002640.
Lee, S.-K., Enfield, D.B., Wang, C., 2007. What drives seasonal onset and decay of the western hemisphere warm pool? J. Clim. 20, 2133–2146, http://dx.doi.org/10.1175/JCLI4113.1.
Lee, S.-K., Wang, C., Mapes, B.E., 2009. A simple atmospheric model of the local and teleconnection responses to tropical heating anomalies. J. Clim. 22 (2), 227–284.
Li, H., Misra, V., 2014. Thirty-two year ocean-atmosphere coupled downscaling of global reanalysis over the Intra-American Seas. Clim. Dyn. 43 (9), 2471–2489, http://dx.doi.org/10.1007/s00382-014-2069-9.
Li, H., Kanamitsu, M., Hong, S.-Y., 2012. California reanalysis downscaling at 10 km using an ocean-atmosphere coupled regional model system. J. Geophys. Res. (Atmos.) 117, D12118, http://dx.doi.org/10.1029/2011JD017372.
Li, H., Kanamitsu, M., Hong, S.-Y., Yoshimura, K., Cayan, D.R., 2013. A high-resolution ocean-atmosphere coupled downscaling of the present climate over California. Clim. Dyn., http://dx.doi.org/10.1007/s00382-013-1670-7.
Li, H., Kanamitsu, M., Hong, S.-Y., Yoshimura, K., Cayan, D.R., Misra, V., Sun, L., 2014. Projected climate change scenario over California by a regional ocean-atmosphere coupled model system. Clim. Change 122 (4), 609–619, http://dx.doi.org/10.1007/s10584-013-1025-8.
Lin, Y., Greatbatch, R.J., Sheng, J., 2009. A model study of the vertically integrated transport variability through the Yucatan Channel: role of Loop Current Evolution and flow compensation around Cuba. J. Geophys. Res. 114, C08003, http://dx.doi.org/10.1029/2008JC005199.
Lindzen, R.S., Nigam, S., 1987. On the role of sea surface temperature gradients in forcing low-level winds and convergence in the tropics. J. Atmos. Sci. 44, 2418–2436.
Liu, H., Wang, C., Lee, S.-K., Enfield, D.B., 2012a. Atlantic warm pool variability in the IPCC AR4 CGCM simulations. J. Clim. 25, 5612–5628, http://dx.doi.org/10.1175/JCLI-D-11-00376.1.
Liu, Y., Lee, S.-K., Muhling, B.A., Lamkin, J.T., Enfield, D.B., 2012b. Significant reduction of the Loop Current in the 21 st century and its impact on the Gulf of Mexico. J. Geophys. Res. 117, C05039, http://dx.doi.org/10.1029/2011JC007555.
Liu, H., Wang, C., Lee, S.-K., Enfield, D.B., 2013. Atlantic warm pool variability in the CMIP5 simulations. J. Clim. 26, 5315–5336, http://dx.doi.org/10.1175/JCLI-D-12-00556.1.
Liu, Y., Lee, S.-K., Enfield, D.B., Muhling, B.A., Lamkin, J.T., Muller-Karger, F., Roffer, M.A., 2015. Potential impact of climate change on the Intra-Americas Seas: part-1. A dynamic downscaling of the CMIP5 model projections. J. Mar. Syst. 148, 56–69, http://dx.doi.org/10.1016/j.jmarsys.2015.01.007.
Locarnini, R.A., Mishonov, A.V., Antonov, J.I., Boyer, T.P., Garcia, H.E., Baranova, O.K., Zweng, M.M., Paver, C.R., Reagan, J.R., Johnson, D.R., Hamilton, M., Seidov, D., 2013. World Ocean Atlas 2013, Volume 1: Temperature. S. Levitus, S., (Ed.), Mishonov, A., (Technical Ed.); NOAA Atlas NESDIS 73, pp. 40.
Mainelli, M., DeMaria, M., Shay, L.K., Goni, G., 2008. Application of oceanic heat content estimation to operational forecasting of recent Atlantic category 5 hurricanes. Weather Forecast. 23 (1), 3–16, http://dx.doi.org/10.1175/2007WAF2006111.1.
Martinho, A.S., Batteen, M.L., 2006. On reducing the slope parameter in terrain following numerical ocean models. Ocean Modell. 13 (2), 166–175, http://dx.doi.org/10.1016/j.ocemod.2006.01.003.
Mellor, G.L., Yamada, T., 1982. Development of a turbulence closure model for geophysical fluid problems. Rev. Geophys. 20, 851–875, http://dx.doi.org/10.1029/RG020i004p00851.
Mellor, G.L., Ezer, T., Oey, L.–Y., 1994. The pressure gradient conundrum of sigma coordinate ocean models. J. Atmos. Ocean Technol. 11 (4), 1126–1134, http://dx.doi.org/10.1175/1520-0426(1994)011<1126:TPGCOS>2.0.CO;2.

Misra, V., Mishra, A., 2016. The oceanic influence on the rainy season of Peninsular Florida. J. Geophys. Res. (Atmos.), http://dx.doi.org/10.1002/2016JD024824, in press.
Misra, V., Chan, S., Wu, R., Chassignet, E., 2009. Air-sea interaction over the Atlantic warm pool in the NCEP CFS. Geophys. Res. Lett. 36, L15702, http://dx.doi.org/10.1029/2009GL038525.
Misra, V., Stroman, A., DiNapoli, S., 2013. The rendition of the Atlantic Warm Pool in the reanalyses. Clim. Dyn. 41, 517–532, http://dx.doi.org/10.1007/s00382-012-1474-1.
Misra, V., Li, H., Kozar, M., 2014. The precursors in the Intra-Americas Seas to seasonal climate variations over North America. J. Geophys. Res. (Oceans) 119 (5), 2938–2948, http://dx.doi.org/10.1002/2014JC009911.
Mo, K.C., Chelliah, M., Carrera, M., Higgins, R.W., Ebisuzaki, W., 2005. Atmospheric moisture transport over the United States and Mexico as evaluated in the NCEP regional reanalysis. J. Hydromet. 6, 710–728.
Moorthi, S., Suarez, M.J., 1992. Relaxed Arakawa-Schubert A parameterization of moist convection for general circulation models. Mon. Weather Rev. 120, 978–1002, http://dx.doi.org/10.1175/1520-0493(1992)120<0978:RASAPO>2.0.CO;2.
Moura, A.D., Shukla, J., 1981. On the dynamics of droughts in northeast Brazil: observations, theory and numerical experiments with a general circulation model. J. Atmos. Sci. 38, 3653–3675.
Rappaport, E.N., Franklin, J.L., Schumacher, A.B., DeMaria, M., Shay, L.K., Gibney, E.J., 2010. Tropical intensity change before U. S Gulf coast landfall. Weather Forecast. 25, 1380–1396, http://dx.doi.org/10.1175/2010WAF2222369.1.
Reynolds, R.W., Smith, T.M., Liu, C., Chelton, D.B., Casey, K.S., Schlax, M.G., 2007. Daily high-resolution-blended analyses for sea surface temperature. J. Clim. 20, 5473–5496, http://dx.doi.org/10.1175/2007JCLI1824.1.
Rossow, W.B., Walker, A.W., Beuschel, D.E., Roiter, M.D., 1996. International Satellite Cloud Climatology Project (ISCCP) Documentation of New Cloud Datasets. WMO/TD-No. 737. World Meteorological Organization, pp. 115 ().
Ruiz-Barradas, A., Nigam, S., 2005. Warm season rainfall variability over the US great plains in observations, NCEP and ERA-40 reanalyses, and NCAR and NASA atmospheric model simulations. J. Clim. 18 (11), 1808–1830, http://dx.doi.org/10.1175/JCLI3343.1.
Schmitz, W.J., Richardson, P.L., 1991. On the sources of the Florida Current. Deep Sea Res. A 38, S379–S409, http://dx.doi.org/10.1016/S0198-0149(12)80018-5.
Shay, L.K., Goni, G.J., Black, P.G., 2000. Effects of a warm oceanic feature on Hurricane Opal. Mon. Weather Rev. 128 (5), 1366–1383, http://dx.doi.org/10.1175/1520-0493(2000)128<1366:EOAWOF>2.0.CO;2.
Shay, L.K., 2009. In: Steele, J., et al. (Eds.), Upper Ocean Structure: Response to Strong Forcing Events. Encyclopedia of Ocean Sciences. , 2nd edition. Elsevier, pp. 192–210, http://dx.doi.org/10.1016/B978-012374473-9.00628-7.
Shchepetkin, A.F., McWilliams, J.C., 2005. The regional oceanic modeling system (ROMS): a split-explicit free-surface, topography-following-coordinate ocean model. Ocean Modell. 9, 347–404.
Sheinbaum, J., Candela, J., Badan, A., Ochoa, J., 2002. Flow structure and transport through the Yucatan Channel. Geophys. Res. Lett. 29 (3), 1040, http://dx.doi.org/10.1029/2001GL013990.
Sikiric, M.D., Janekovic, I., Kuzmic, M., 2009. A new approach to bathymetry smoothing in sigma-coordinate ocean models. Ocean Modell. 29 (2), 128–136, http://dx.doi.org/10.1016/j.ocemod.2009.03.009.
Tanimoto, Y., Xie, S.-P., 2002. Inter-hemispheric decadal variations in SST, surface wind, heat flux and cloud cover over the Atlantic Ocean. J. Meteorol. Soc. Jpn. 80, 1199–1219.
Tiedtke, M., 1983. The sensitivity of the time-mean large-scale flow to cumulus convection in the ECMWF model. In: Proceedings of ECMWF Workshop on Convective in Large-scale Models. European Centre for Medium-Range Weather Forecasts, Reading, United Kingdom, pp. 297–316.
Umlauf, L., Burchard, H., 2003. A generic length-scale equation for geophysical turbulence models. J. Mar. Res. 61 (2), 235–265, http://dx.doi.org/10.1357/002224003322005087.
Wang, C., Enfield, D.B., 2001. The tropical western hemisphere warm pool. Geophys. Res. Lett. 28, 1635–1638.
Wang, C., Enfield, D.B., 2003. A further study of the tropical western hemisphere warm pool. J. Clim. 16 (10), 1476–1493, http://dx.doi.org/10.1175/1520-0442-16.10.1476.
Wang, C., Enfield, D.B., Lee, S.–K., Landsea, C., 2006. Influences of the Atlantic warm pool on Western Hemisphere summer rainfall and Atlantic hurricanes. J. Clim. 19 (12), 3011–3028, http://dx.doi.org/10.1175/JCLI3770.1.
Wang, C., Lee, S.-K., Enfield, D.B., 2007. Impact of the Atlantic warm pool on the summer climate of the Western Hemisphere. J. Clim. 20, 5021–5040.
Wang, C., Lee, S.–K., Enfield, D.B., 2008a. Climate response to anomalously large and small Atlantic Warm pools during the summer. J. Clim. 21 (11), 2437–2450, http://dx.doi.org/10.1175/2007JCLI2029.1.
Wang, C., Lee, S.-K., Enfield, D.B., 2008b. Atlantic warm pool acting as a link between atlantic multidecadal oscillation and atlantic tropical cyclone activity. Geochem. Geophys. Geosyst. 9 (5), Q05V03, http://dx.doi.org/10.1029/2007GC001809.
Zhang, L., Wang, C., Xiu, L., 2012. Low frequency modulation of the Atlantic warm pool by the Atlantic multidecadal oscillation. Clim. Dyn. 39 (7), 1661–1671, http://dx.doi.org/10.1007/s00382-011-1257-0.